Estimation and compensation of frequency sweep nonlinearity in FMCW radar

by

Kurt Peek

Picture: www.thalesgroup.com

A thesis submitted in partial fulfillment

Of the requirements for the degree of

MASTER OF SCIENCE in APPLIED MATHEMATICS

Supervisors: Gjerrit Meinsma, Anton Stoorvogel

Table of Contents

Abstract

One of the main issues limiting the range resolution of linear frequency-modulated continuous-wave (FMCW) radars is nonlinearity of frequency sweep, which results in degradation of contrast and range resolution, especially at long ranges. Two novel, slightly different, methods to correct for nonlinearities in the frequency sweep by digital post-processing of the deramped signal were introduced independently by Burgos-Garcia et al. (Burgos-Garcia, Castillo et al. 2003) and Meta et al. (Meta, Hoogeboom et al. 2006). In these publications, however, no formal proof of the techniques was given, and no limitations were described. In this thesis, we prove that the algorithm of Meta is exact for temporally infinite chirps, and remains valid for finite chirps with large time-bandwidth products provided the maximum frequency component of the phase error function is sufficiently low. It is also shown that the algorithm of Meta reduces to that of Burgos-Garcia in this limit. A digital implementation of the method is described. We also propose a novel method to measure the systematic phase errors which are required as input to the compensation algorithm. The applicability of this technique to the field of optical frequency domain reflectometry (OFDR) is noted.

1   Introduction

Frequency-modulated continuous-wave (FMCW) radars provide high range measurement precision and high range resolution at moderate hardware expense (Griffiths 1990; Stove 1992). Moreover, the spreading of the transmitted power over a large bandwidth provides makes FMCW radar difficult to detect by intercept receivers, providing it with stealth in military applications. In the last two decades, Thales Netherlands has developed a family of silent radars for air surveillance, coastal surveillance, navigation, and ground surveillance based on FMCW technology.

In FMCW radar, the range to the target is measured by systematically varying the frequency of a transmitted radio frequency (RF) signal. Typically, the transmitted frequency is made to vary linearly with time; for example, a sawtooth or triangular frequency sweep is implemented. The linear variation of frequency with time is referred to as a *chirp*, *frequency sweep*, or *frequency ramp*. Figure 1 shows a time-frequency plot of a linear sawtooth FMCW transmit signal and its corresponding amplitude.
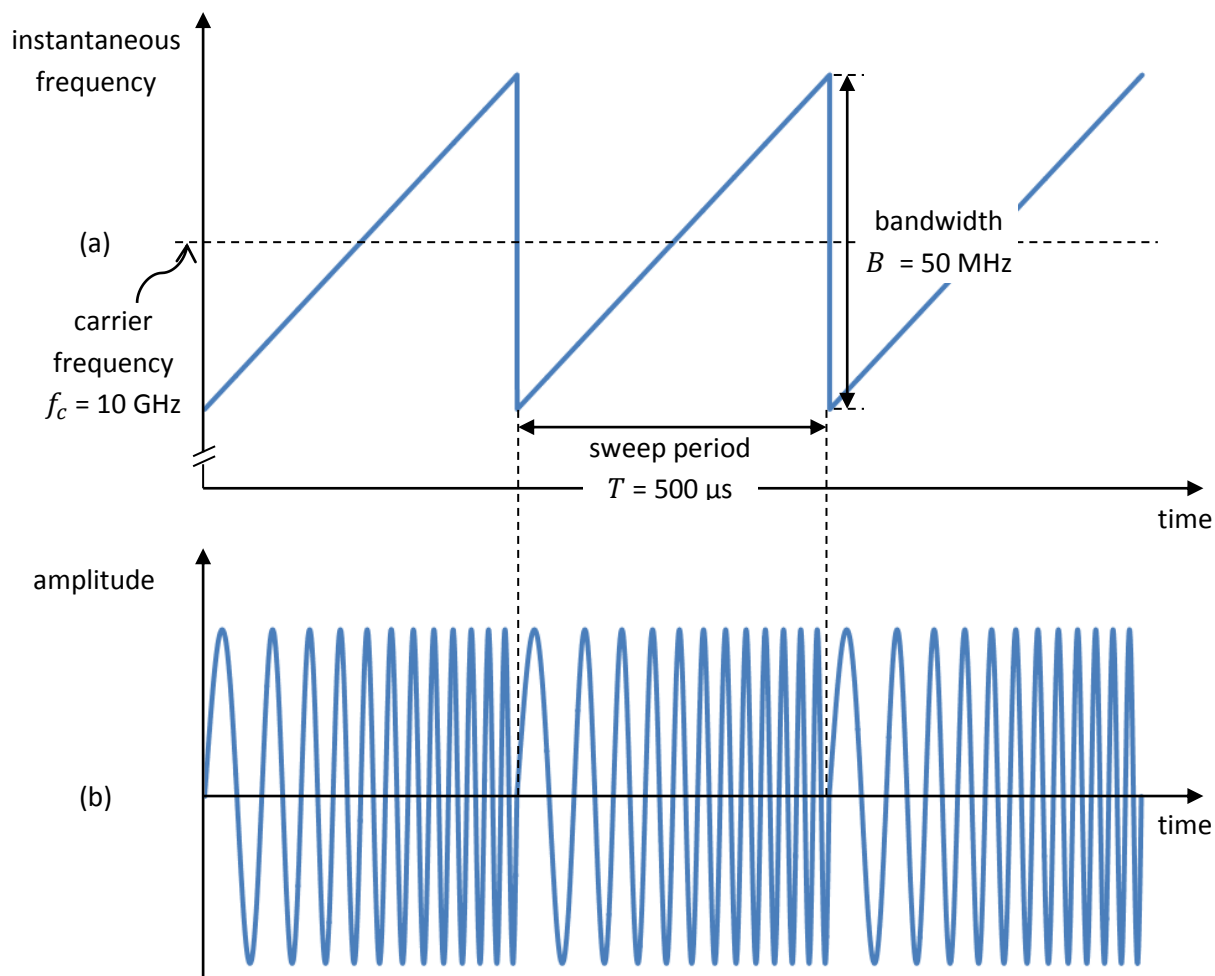
Figure 1 (a) Time-frequency plot of a FMCW transmit signal with carrier frequency f_c, sweep period T, and bandwidth[1] B. Typical parameters are f_c = 10 GHz, T = 500 µs, and B = 50 MHz. (b) Time-amplitude plot of a transmitted FMCW signal (not with the parameters listed above).

The frequency sweep effectively places a "time stamp" on the transmitted signal at every instant, and the frequency difference between the transmitted signal and the signal returned from the target (i.e. the reflected or received signal) can be used to provide a measurement of the target range, as illustrated in Figure 2. This process is called *dechirping* or *deramping*, and the frequency of the dechirped signal is called the *beat* or *intermediate frequency* (IF) signal.

---

[1] The term 'bandwidth' is often used in this context to refer to the total excursion of the instantaneous frequency during one the sweep period. The FMCW signal is not bandlimited in the mathematical sense of the word; however, for large time-bandwidth products it is approximately bandlimited.
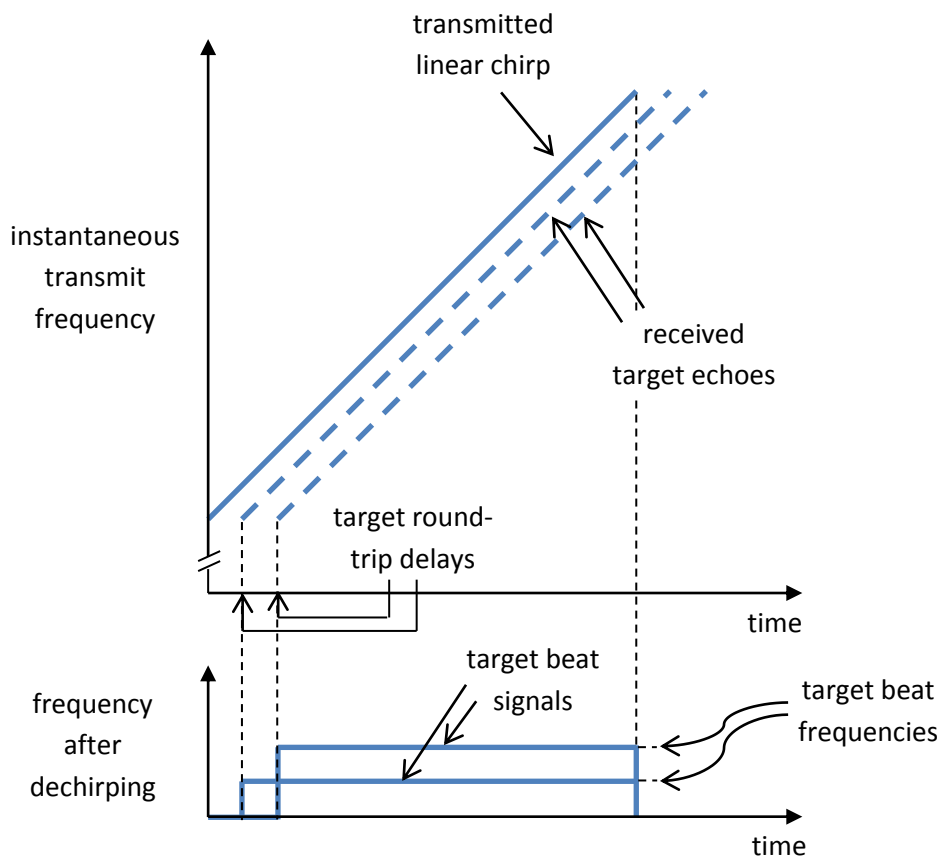
Figure 2 Principle of FMCW range measurement. (a) Time-frequency plots of the transmitted chirp (solid line) and the echoes from two 'point' targets (dashed lines), delayed by their respective two-way propagation delays to the target and back. (b) Time-frequency plots of the frequency difference, or 'beat frequency', between the transmitted and received chirps. The beat frequency is observed during portion of the sweep period in which the transmitted and received signals overlap.

As seen from Figure 2, the target transit time and target beat frequency are directly proportional, and their proportionality constant is equal to the *chirp rate* (i.e., the ratio between the bandwidth and the sweep period) of the transmitted chirp. Hence, the target transit time – and thus, the target range – can be inferred by a measurement of the beat frequency.

The beat frequency is generated in the receiver of the FMCW radar by a *mixer*[2] or 'multiplier' as illustrated in **Error! Reference source not found.**. The local oscillator (LO) port of the mixer is fed by a portion of the transmit signal[3], while the radio frequency (RF) port is fed by the target echo signal from the receive antenna. As explained in more detail in Section 2.1.3, the output of the mixer, called the *intermediate frequency* (IF) signal, has a phase which (after low-pass filtering) is the

---

[2] A *mixer* is a three-port device that uses a nonlinear or time-varying element to achieve frequency conversion (Pozar 2005). In its down-conversion configuration, it has two inputs, the *radio frequency* (RF) signal and the *local oscillator* (LO) signal. The output, or *intermediate frequency* (IF) signal, of an idealized mixer is given by the product of RF and LO signals.

[3] This is the *homodyne* receiver architecture, in which the local oscillator signal is provided by the transmitter itself. Alternatively, the local oscillator can be generated separately and triggered at an appropriate instant; this is commonly referred to as *stretch processing* (Caputi 1971). Stretch processing has the disadvantage of the additional complexity of another oscillator. Receiver noise effects will also be greater because of the independence of the phase noise of the separate oscillators (Piper 1993).

difference of the phases of the LO and RF signals. Hence, its frequency is the 'beat 'frequency described above. The beat signal is passed to a spectrum analyzer, which is a bank of filters used to resolve targets in to range bins. Typically, the spectrum analyzer is implemented as an analog-to-digital converter (ADC) followed by a processor based on the fast Fourier transform (FFT).
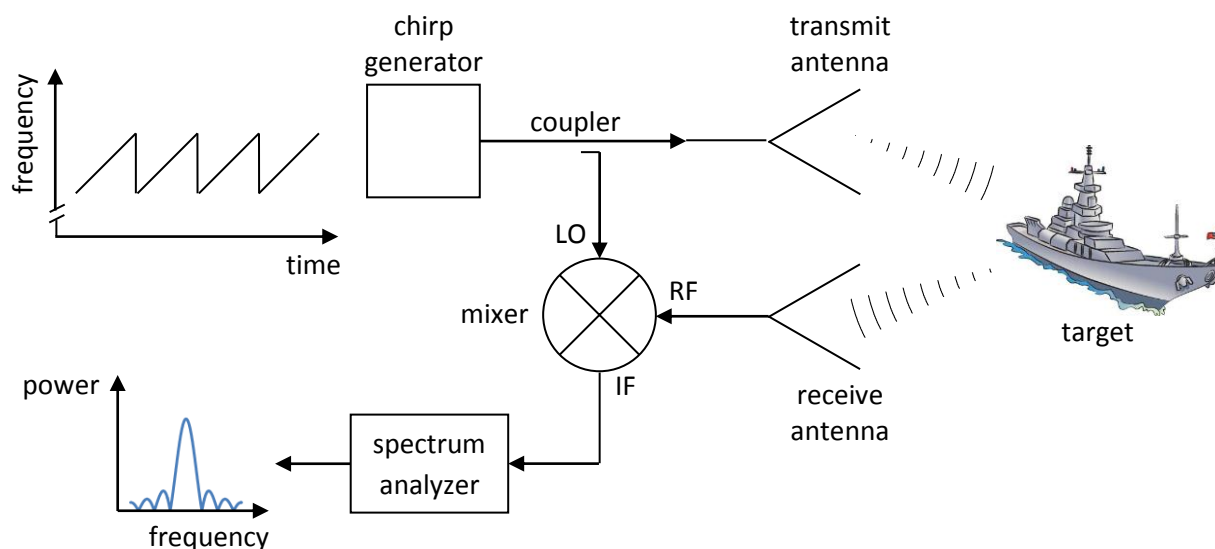
Figure 3 Simplified block diagram of a homodyne FMCW radar transceiver. A chirp generator generates a linear sawtooth FMCW signal (left, upper inset) which is radiated out to the target scene by a transmit antenna. A portion of the transmitted signal is coupled to the local oscillator (LO) port of a mixer. The target echo received by a separate receive antenna is fed to the radio frequency (RF) port of the mixer. The mixer output at intermediate frequency (IF) is fed to a spectrum analyzer. The output of the spectrum analyzer for a single target is a 'sinc' function centered at the target beat frequency (left, lower inset).

The performance of a linear FMCW radar is strongly dependent on the linearity of the transmitted signal. Deviation of the instantaneous frequency from a linear one – or equivalently, deviation of the phase from a quadratic one – causes 'smearing' of the target beat signal in frequency, resulting in spurious "ghost" targets and degradation of the signal-to-noise ratio (SNR). The effect is usually worse at larger range, where phases of the transmitted and received signals are more de-correlated. This effect is illustrated in Figure 4
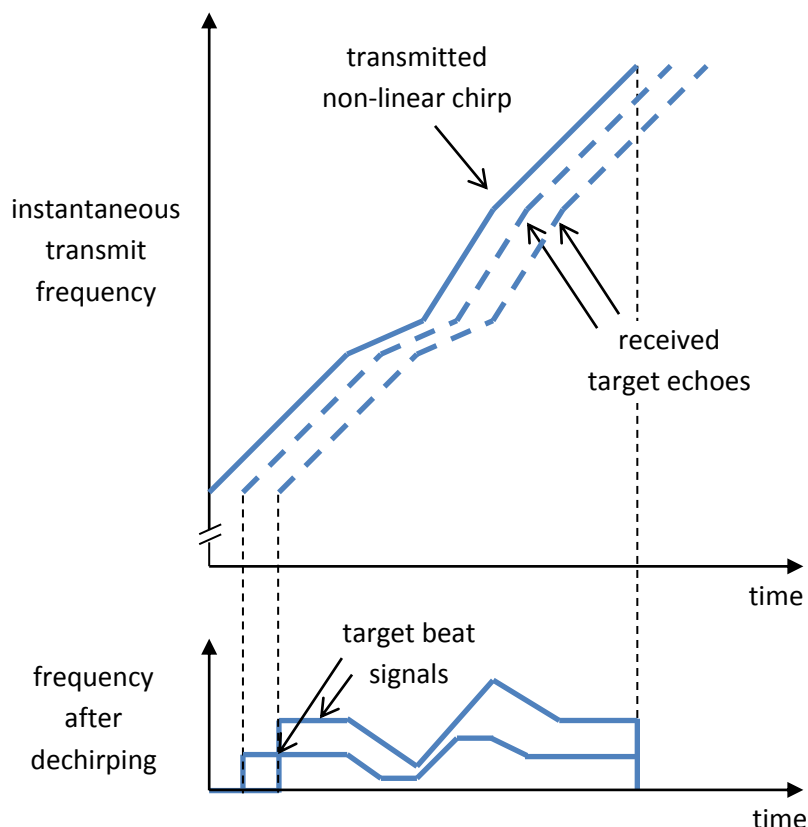
Figure 4 FMCW range measurement with non-linear chirps. Due to the nonlinearity of the transmitted chirp, the target beat signals are 'spread' or 'smeared' in frequency. The degradation worsens with increasing range.

A number of different approaches have thus been adopted over the years with the aim of improving the frequency sweep linearity of FMCW radar systems. These can be categorized in 'hardware' techniques, which attempt to generate more linear chirps, and 'software' techniques, which use signal processing to compensate the effects of the non-linearity *a posteriori*. Although our focus in this report is on the latter, it is instructive to discuss shortly the former.

1.1 'Hardware' sweep linearization

Firstly, attempts have been made to produce chirp generators that are inherently linear. One way is to apply a linear sawtooth current signal to a Yttrium Iron Garnet (YIG)-tuned oscillator, which is a current-controlled oscillator (CCO) with an inherently linear tuning characteristic. This scheme is representative of the world's first mass-produced FMCW navigation radar: the Pilot FMCW radar, developed by Philips Research Laboratories in 1988 and marketed by its subsidiaries PEAB in Sweden and Hollandse Signaalapparaten in the Netherlands (Pace 2009). The typically attainable sweep linearity of 0.1% still limits the obtainable range resolution in FMCW applications, however, and the switching speed is low, of the order of milliseconds.

In FMCW transmitters employing voltage-controlled oscillators (VCOs), the most common 'hardware' method used for frequency sweep linearization is closed loop feedback. The closed loop feedback technique has been implemented in a variety of ways, but they are all based on creating an artificial target which generates a "beat" frequency when mixed with a reference signal. In a perfectly linearized FMCW radar a fixed range target would produce a constant "beat" frequency.

Therefore, in a practical FMCW radar, if the "beat" frequency drifts from the desired constant frequency value, an error signal can be generated to fine-tune the VCO to maintain a constant "beat" frequency. This feedback technique can be implemented at the final RF frequency of the radar or at a lower, down-converted frequency. Waveforms having sweep linearity[4] better than 0.05% have been demonstrated {Fuchs, 1996 #181} but, unless the system is very well designed, the technique can be prone to instabilities and is typically limited in bandwidth to about 600 MHz. Also, because the VCO is modulated directly, the phase noise of the resultant transmit signal can be compromised (Beasley 2009).

The use of a direct digital synthesizer (DDS) offers quite a cost-effective solution, however the transmitted bandwidth is still limited compared to the one obtained by directly sweeping a VCO. Moreover, nonlinearity can still be caused by group delay in subsequent filters (Perez-Martinez, Burgos-Garcia et al. 2001).

Method	References	Advantages	Disadvantages
Free-running YIG oscillator	PILOT FMCW radar, {Beasley, 2010 #318}	Low phase noise, sweep linearity of 0.1% attainable	Slow modulation speed, power-hungry, drifts with temperature
VCO with closed-loop feedback	{Fuchs, 1996 #181}	Sweep linearity better than 0.05%	Prone to instabilities, typically limited in bandwidth to about 600 MHz
Direct digital synthesis (DDS)	{Goldberg, 2006 #212}	Linear chirp generated to digital precision	Limited bandwidth, requires upconversion, group delay introduced through filtering further down the transmission chain

Table 1 Techniques for generating linear FMCW chirps.

Table 1 summarizes techniques for generating linear chirps with their advantages and disadvantages. In summary, each of the 'hardware' techniques has its limitations.

1.2 'Software' linearization techniques

As an interesting alternative to these hardware techniques, a software-based linearization method using a transmission measurement through a reference delay line has been reported in both FMCW radar (Fuchs, Ward et al. 1996; Vossiek, Kerssenbrock et al. 1997) and, more recently, in optical frequency-domain reflectometers (OFDR) (Ahn, Lee et al. 2005; Saperstein, Alic et al. 2007). However, this technique assumes that the phase error can be linearized on the target delay interval, which limits its validity to short range intervals {Meta, 2007 #46}.

Relatively recently, Burgos-Garcia et al. {Burgos-Garcia, 2003 #341} and Meta et al. {Meta, 2007 #46} have reported on novel processing methods which employ a "residual video phase" (RVP) or "deskew" filter. These methods, which operate directly on the deramped data, correct the

---

[4] Sweep linearity is defined as the maximum deviation in frequency from a linear chirp as a percentage of the swept bandwidth.

nonlinearity effects for the whole range profile at once, and are based only on the assumption that the transmitted chirp has a large time-bandwidth product.

1.3   This thesis

The algorithms proposed by Burgos-Garcia et al. {Burgos-Garcia, 2003 #341} and Meta et al. {Meta, 2007 #46} are actually slightly different. Further, they are presented based on heuristic reasoning; no formal proof is given, and no limitations of the algorithm are mentioned.

This thesis makes three main contributions to knowledge:

(1) We give a proof of both Meta's "wideband" and Burgos-Garcia's "narrowband" variations of the phase error compensation algorithm. It is shown that the algorithm of Meta reduces to that of Burgos-Garcia in the special case that the error frequency components are sufficiently low. Further, our analytical results indicate that the original algorithm as presented by Meta {Meta, 2006 #340}{Meta, 2007 #46} contains a sign error. Finally, we discuss issues which arise when applying the algorithm to time-limited chirps, which have not been discussed previously.

(2) We implement both phase error compensation algorithms in MATLAB and demonstrate their effectiveness. (In {Burgos-Garcia, 2003 #341} and {Meta, 2007 #46}, no detail was given on the digital implementation of the algorithm). The results of our simulation are inconclusive, however, as to whether there is a minus sign error in Meta's derivation or not. Further improvements to the simulation algorithm, which involve taking into account the "edge effects" due to the time-limited nature of the chirps, are proposed.

(3) We propose a novel method for determining the phase errors using measurements from targets at different reference delays, based on the synthesis problem of a function from its ambiguity function as discussed by Wilcox {Wilcox, 1991 #391}. The novel method could have advantages over known methods, which use just a single reference delay.

The organization of this thesis is as follows. In Chapter 2, we discuss the theory of operation of FMCW radar in more mathematical detail. In Chapter 3, we derive both variations of the phase error compensation algorithm analytically and address the issues mentioned above in point (1). In Chapter 0, we perform a simulation of the algorithms and demonstrate their effectiveness. In Chapter 5, we discuss the estimation of phase errors, which are required as input for the algorithm. Finally, in Chapter 6, we wrap up with our conclusions and discussion.

2 Theory of operation of FMCW radar

This chapter presents a tutorial review of the basic principles of FMCW (frequency modulated continuous wave) radars. The material to follow is on *homodyne* FMCW radar, i.e., CW radar in which a microwave oscillator is frequency-modulated and serves as both transmitter and local oscillator (Skolnik 2008). The effect of frequency sweep nonlinearity is also discussed.

An outline of this chapter is as follows. In Section 2.1, we present an analytical model of the generation of the target range profile by a FMCW transmitting ideal linear chirps. In Section 2.2, we discuss how its performance is affected by sinusoidal frequency sweep nonlinearities.

2.1 Analytical model of a FMCW radar

In this section, we explain the principle FMCW range measurement in more mathematical detail. In Section 2.1.1, we formulate an expression for the transmitted signal. In Section 2.1.2, we construct a model for the received signal. In Section 2.1.3, we explain the generation of the 'dechirped', 'deramped', or 'beat' signal. Of particular importance for the algorithm to be described is the use of 'coherent detection' to obtain complex samples of this signal. Finally, in Section 2.1.4, we discuss the spectrum of the beat signal or 'video signal', which is used to visualize the target scene.

2.1.1 Transmitted signal

We select a 100% duty factor signal whose frequency sweeps upward, linearly, over one sweep repetition interval T. Using a complex number representation (Jakowatz, Wahl et al. 1996), the transmitted signal $\tilde{s}_{TX}$ with unity amplitude can be expressed as the real part of

$$\tilde{s}_{TX}(t) = \sum_{n=-\infty}^{\infty} s_{TX}(t - nT), \tag{2.1}$$

where $s_{TX}(t)$ is the linear chirp pulse

$$s_{TX}(t) = \text{rect}\left(\frac{t}{T}\right) \exp\left[j2\pi\left(f_c t + \frac{1}{2}\alpha t^2\right)\right] \equiv \text{rect}\left(\frac{t}{T}\right) \exp[j\phi_{TX}(t)]. \tag{2.2}$$

Here t represents the time variable, $j = \sqrt{-1}$ the imaginary unit, f_c the chirp's center frequency, and α its frequency sweep rate, and $\text{rect}(\cdot)$ is the *rectangular function* given by

$$\text{rect}(x) = \begin{cases} 1, & |x| < \dfrac{1}{2}, \\[2mm] \dfrac{1}{2}, & |x| = \dfrac{1}{2}, \\[2mm] 0, & |x| > \dfrac{1}{2}. \end{cases} \tag{2.3}$$

We assume here that the transmit signal is periodic, and hence phase-coherent from one sweep to the next[5].

---

[5] By sweep-to-sweep coherence, we mean that there is a fixed relationship between the phase in one sweep and the next, i.e., $\phi_{TX}(t + T) - \phi_{TX}(t) = $ constant. FMCW radars having this property are called *coherent*, and have several advantages. For example, coherent systems allow *Doppler processing* (Barrick 1973) to determine information on the velocity of detected targets. Furthermore, *coherent integration* over N

Since the instantaneous frequency, $f_{TX}(t)$, is the derivative of the phase (Carson 1922), we have

$$f_{TX}(t) = \frac{1}{2\pi}\frac{d\phi_{TX}}{dt} = f_c + \alpha t. \tag{2.4}$$

Thus it can be seen that the frequency excursion over one sweep repetition interval is $\alpha T = B$, the chirp bandwidth. The instantaneous frequency of the transmit signal is plotted in Figure 5(a) as the solid line.
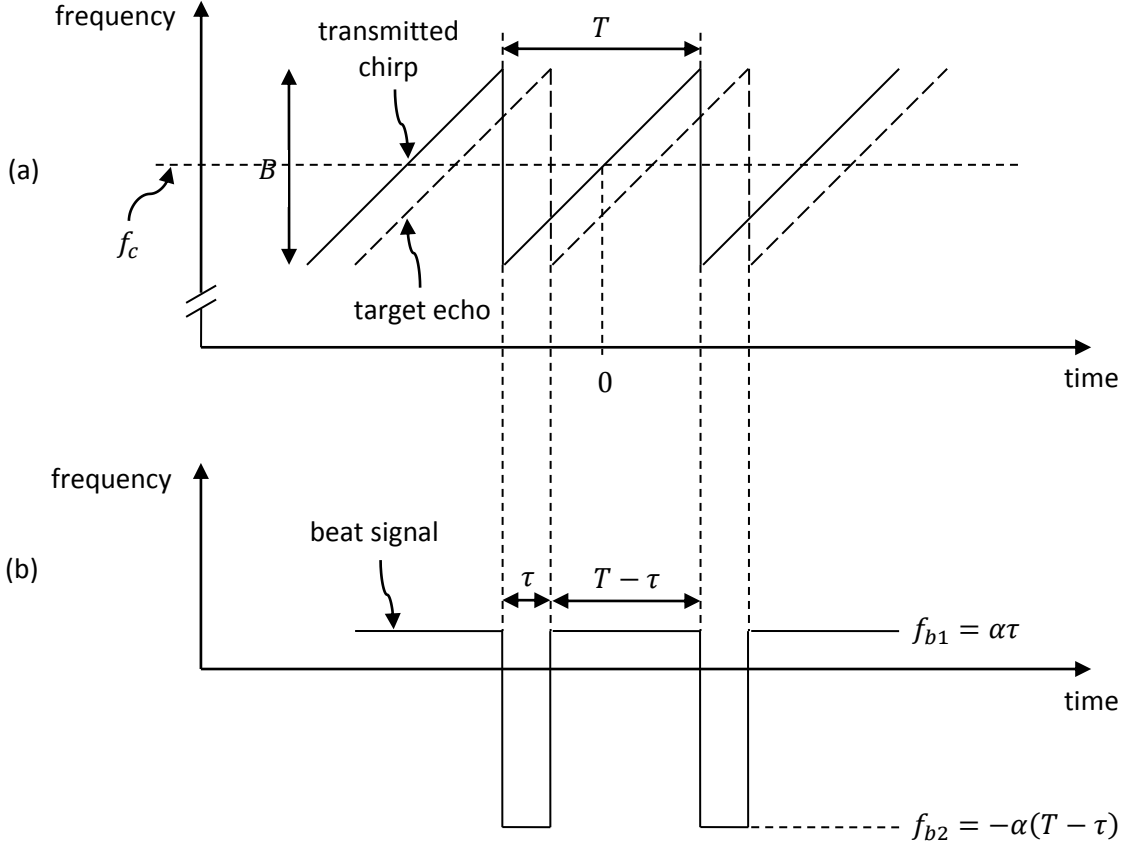
Figure 5 Time-frequency plots of (a) the transmitted (solid line) and received (dashed line) signals, and (b) the intermediate frequency (IF) signal. The IF alternates between two distinct tones: $f_{b1} = \alpha\tau$ for intervals of duration $T - \tau$ and $f_{b2} = -\alpha(T - \tau)$ for intervals of duration τ, where $\alpha = B/T$ is the frequency sweep rate. Typical chirp parameters for an FMCW navigation radar are f_c = 10 GHz, B = 50 MHz, and T = 500 μs.

2.1.2   Received signal

After transmission of the radar signal through the transmit antenna, the radar waveform propagates to the target scene, and part of the energy is scattered back to the radar's receive antenna. In the following analytical development, we assume that the target scene consists of a single stationary 'point' target such that the echo signal $\tilde{s}_{RX}(t)$ is simply a delayed replica of the transmit signal:

$$\tilde{s}_{RX}(t) = \tilde{s}_{TX}(t - \tau), \tag{2.5}$$

where τ is the two-way propagation delay given by

---

frequency sweeps improves the signal-to-noise ratio (SNR) by a factor of N. This should be contrasted with the SNR increase of $\sqrt{N}$ typically obtained using incoherent integration of N frequency sweeps (Beasley 2009).

$$\tau = \frac{2R}{c}, \tag{2.6}$$

where R is the range of the stationary 'point' target, and c is the propagation velocity.

If we assume that the radar receiver is a *linear* system[6], then the range profile obtained from a general target scene can be obtained by superposition of the range profiles of the individual targets. Thus, the modeling a 'point' target is merely a convenient way to separate algorithm and hardware effects from target and interference phenomenology.

To obtain an expression for the received signal corresponding to a single sweep of the transmitted signal, we insert (2.2) into (2.5) to find

$$s_{RX}(t) = \text{rect}\left(\frac{t-\tau}{T}\right) \exp\left[j2\pi\left(f_c(t-\tau) + \frac{1}{2}\alpha(t-\tau)^2\right)\right] \equiv \text{rect}\left(\frac{t-\tau}{T}\right) \exp[j\phi_{RX}(t)]. \tag{2.7}$$

The instantaneous frequency of the periodic repetition of s_{RX}, $\tilde{s}_{RX}$, is plotted in Figure 5(a) as the dashed line.

2.1.3   Dechirped signal

As explained in the Introduction, upon reception the received signal is correlated with the transmitted signal through a mixing process. In this section, we explain in more detail the mixing process and subsequent digitization (Section 2.1.3.1) and the retrieval of phase information by a method called in-phase (I) / quadrature (Q) demodulation (Section 2.1.3.2).

2.1.3.1   Mixing process

Now after bandpass filtering to reject wideband noise and radio frequency (RF) amplification, the received signal is 'dechirped' or 'deramped' by 'mixing' or 'beating' it together with a replica of the transmitted signal in a mixer as illustrated in Figure 6. The resulting signal will contain a product term $G \cos\phi_{TX} \cos\phi_{RX}$, where G is a constant accounting for the voltage conversion loss of the mixer, and other higher-order products. In general, only the lowest-order product will have significant amplitude. The product may be expanded as a sum, namely

$$\frac{G}{2}[\cos(\phi_{TX} - \phi_{RX}) + \cos(\phi_{TX} + \phi_{RX})].$$

The phase-sum term represents an oscillation at twice the carrier frequency, which is generally filtered out either actively, or more usually in radar systems because it is beyond the cut-off frequency of the mixer and subsequent receiver components (Brooker 2005)[7]. We are thus

---

[6] In practice, the FMCW receiver is not ideally linear; for example, mixer and a high-gain pre-amplifier which follows the receive antenna will generate harmonic distortion and intermodulation distortion (IMD). These are separate hardware issues however, however; here, we are concerned with errors arising from nonlinearity of the frequency sweep.

[7] FMCW radars sometimes employ a so-called *image reject mixer* (IRM) instead of a conventional one to generate the IF signal. The FMCW radar using a conventional mixer suffers a 3 dB loss in signal-to-noise ratio (SNR) due to the addition of noise at the RF image frequency to the RF noise when both are down-converted to near-zero IF. This effect cannot easily be removed by RF filtering because of the closeness of the RF and image frequencies, but can be removed if an IRM is used (Willis and Griffiths 2007).

interested in the function $\frac{G}{2}\cos(\phi_{TX} - \phi_{RX})$, which is called the 'dechirped', 'deramped', 'beat', or 'intermediate frequency' (IF) signal. The IF signal with unity amplitude (we do not consider amplitude variations in this derivation) is thus

$$\cos(\phi_{IF}) \equiv \cos(\phi_{TX} - \phi_{RX}). \tag{2.8}$$
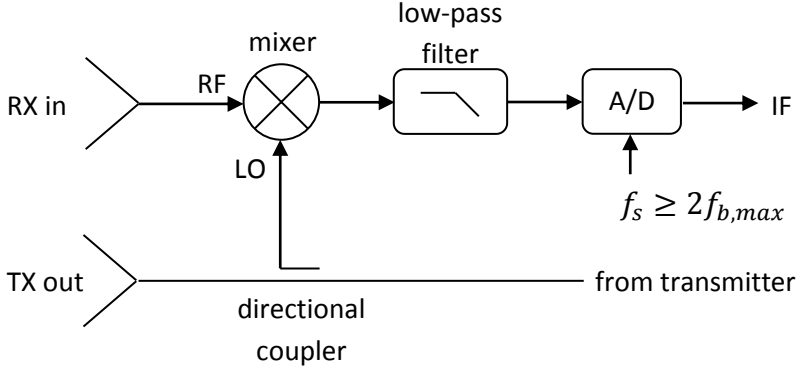
Figure 6 Simplified block diagram of a homodyne FMCW transceiver. The received (RX) signal is fed to the radio frequency (RF) port of a mixer, while a portion of the transmit (TX) signal is coupled to the local oscillator (LO) port. The mixer output is low-pass filtered to obtain the desired intermediate frequency (IF) signal, which is digitized by an analog-to-digital (A/D) converter at a rate f_s of at least twice the maximum beat frequency $f_{b,max}$.

A complex representation of the IF signal resulting from a single pulse of the transmitted signal is obtained by Inserting (2.2) and (2.7) into (2.8), a single pulse of the IF signal can be expressed as the real part of

$$s_{IF}(t) \equiv s_{TX}(t)s_{RX}^*(t)$$
$$= \text{rect}\left(\frac{t}{T}\right)\text{rect}\left(\frac{t-\tau}{T}\right)\exp\left[j2\pi\left(f_c t + \frac{1}{2}\alpha t^2 - f_c(t-\tau) - \frac{1}{2}\alpha(t-\tau)^2\right)\right]$$

or, simplifying,

$$s_{IF}(t) = r(t)\exp\left[j2\pi\left(f_c\tau + \alpha\tau t - \frac{1}{2}\alpha\tau^2\right)\right], \tag{2.9}$$

where the beat signal envelope $r(t)$ is given by

$$r(t) = \begin{cases} 1, & -T/2 + \tau < t < T/2, \\ 0, & \text{otherwise.} \end{cases} \tag{2.10}$$

During the remaining part of the sweep period, on the interval $[-T/2, -T/2 + \tau]$, the received signal corresponds to the transmitted signal during the previous sweep. Therefore, the mixer output will be offset by the sweep width, B, as illustrated in Figure 5(b). B is much greater than the signal frequency and the mixer output for $-T/2 < t < -T/2 + \tau$ will therefore be filtered and rejected. Hence, for $-T/2 < t < -T/2 + \tau$, the IF signal will be a transient pulse. If a digital data system is used to observe the mixer output, the sampling can be delayed at the start of each sweep so the retrace effects of the local oscillator returning to $f_c - B/2$ are simply omitted (Strauch 1976).

Let us consider the three terms that comprise the phase of the IF signal (2.9):

- $f_c \tau$ is the total number of cycles of f_c that occur during the round trip propagation time for the target[8].
- $\alpha \tau t$ is a term increasing linearly with the time t, and represents the target beat frequency $f_b = \alpha \tau$.
- $-\alpha \tau^2/2$ is a range-dependent phase term. In the synthetic aperture radar (SAR) literature, it is called the *residual video phase* (Carrara, Goodman et al. 1995). As we will see, this term plays a key role in the phase compensation algorithm.

The third term, the residual video phase, will prove to play a crucial role in the phase error compensation algorithm.

2.1.3.2   *Retrieval of in-phase and quadrature components*
The mixing process described above produces a real voltage signal

$$\mathcal{Re}\{s_{IF}\} = \cos(\phi_{IF}), \tag{2.11}$$

where s_{IF} is given by (2.9). After analog-to-digital conversion as described in Section 2.1.4, this appears digitally as an array of real numbers. Ideally, however, we would like to obtain the complex representation s_{IF} itself, which we refer to as the *baseband* signal. Knowledge of the baseband signal has a number of advantages:

- It allows positive and negative frequencies to be recovered separately. As pointed out by Gurgel and Schlick (Gurgel and Schlick 2009), in the case of a linear chirp with increasing frequency (a positive chirp), the beat frequency defined by (2.9) will always be positive. Therefore, a 3 dB gain in signal-to-noise ratio (SNR) can be obtained by avoiding the aliasing noise from the "unused" negative side of the spectrum.
- By converting the IF signal into baseband form, a simple multiplication of each sample with the appropriate complex number achieves any desired phase adjustment of that sample.

The latter point is an essential part of the phase compensation algorithm to be described in the following chapter. Thus, it is desirable to obtain the beat signal in complex form, but how is this done?

Mathematically, there are actually two ways of obtaining a complex representation of a signal from a real one {Boashash, 1992 #363}:

1) The "real plus imaginary quadrature" representation, in which the cosine in (2.11) is replaced by a complex exponential. The real and imaginary parts of this complex exponential are called the *in-phase* (I) and *quadrature* (Q) components, respectively:

$$I = \mathcal{Re}\{s_{IF}\} = \cos\phi_{IF}, \qquad Q = \mathcal{Im}\{s_{IF}\} = \sin\phi_{IF}. \tag{2.12}$$

---

[8] Incidentally, for coherent FMCW radar applications such as Doppler processing and coherent integration, this term should ideally be constant for all processed sweeps. However, because this term typically is very large compared to the other terms, this places very stringent requirements on the frequency stability of the chirp generator (Strauch 1976).

2) The *analytic signal* representation, in which the negative frequency components of (2.11) are discarded and the positive ones multiplied by a factor two. (This is equivalent to adding to (2.11) an imaginary part equal to its *Hilbert transform*).

As shown by Nuttall {Nuttall, 1966 #231}, the two approaches are only equivalent if the "real plus imaginary quadrature" representation is spectrally one-sided. In our case, it is "real plus imaginary quadrature" representation that corresponds exactly with the desired baseband signal.

The conversion of real signals to a baseband representation, $I + jQ$, is performed by a so-called *I/Q demodulator*, also known as a *quadrature detector*, *synchronous detector*, or *coherent detector* (Skolnik 2008). Coherent detection can be performed both before and after digitization.

Figure 7 illustrates the classical analog implementation of an I/Q demodulator. The received signal $\cos \phi_{RX}$ is split and fed to a pair of mixers or analog multipliers. The transmit signal $\cos \phi_{TX}$, obtained from the transmit chain by a directional coupler, is input to a *quadrature splitter*, also known as a *quadrature hybrid* or *90° hybrid* (Pozar 2005). Ideally, this results in two outputs: one proportional to $\cos \phi_{TX}$ in phase with the input, and the other proportional to $\sin \phi_{TX}$ at phase quadrature to the input. These outputs are fed to LO ports of two mixers and mixed (multiplied) with the received signal, $\cos \phi_{RX}$. As in Section 2.1.3.1, the mixer products can be expanded into phase-sum and phase-difference terms via the trigonometric relations

$$\cos(\phi_{RX}) \cos(\phi_{TX}) = \frac{1}{2}[\cos(\phi_{TX} + \phi_{RX}) + \cos(\phi_{TX} - \phi_{RX})]$$

and

$$\cos(\phi_{RX}) \sin(\phi_{TX}) = \frac{1}{2}[\sin(\phi_{TX} + \phi_{RX}) + \sin(\phi_{TX} - \phi_{RX})].$$

The sum-frequency components are at approximately twice the RF frequency and easily filtered. What remains are the terms $\cos(\phi_{TX} - \phi_{RX}) = \cos(\phi_{IF})$ and $\sin(\phi_{TX} - \phi_{RX}) = \sin(\phi_{IF})$. These are exactly the in-phase (I) and quadrature (Q) components of the IF signal, respectively, and can be combined to obtain the full baseband signal $s_{IF} = \exp(j\phi_{IF})$ as desired.
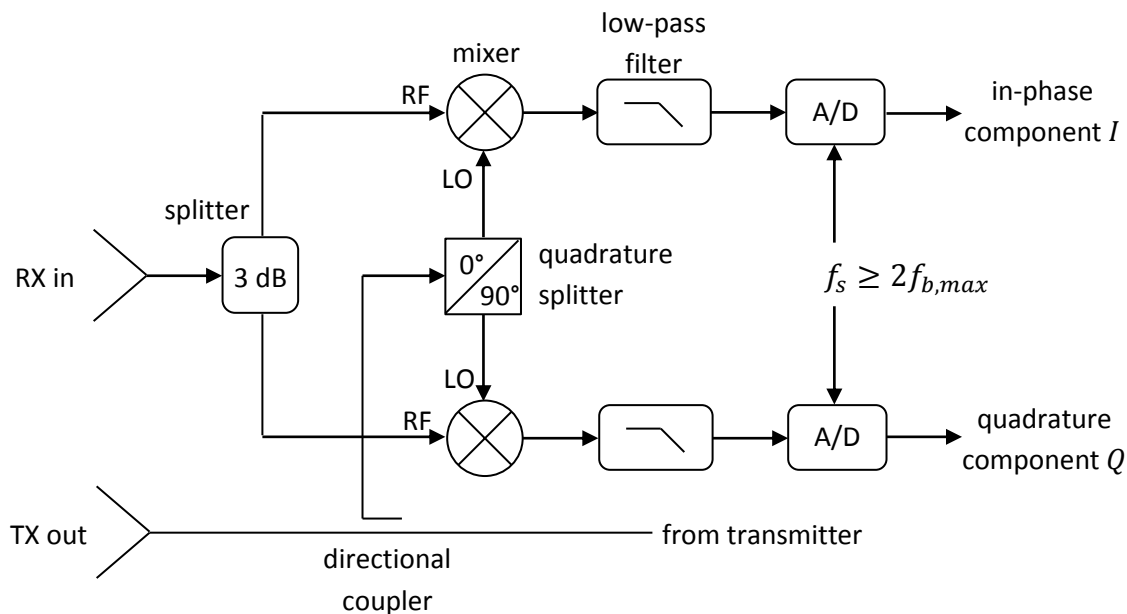
Figure 7 Simplified block diagram of an analog I/Q demodulator for a homodyne FMCW system. The received signal is applied to a 3-dB power splitter, the two outputs of which are applied to the RF ports of (double-balanced) mixers. The local oscillator (LO) ports are driven by two samples of the transmit signal, the two components being in phase quadrature. The resulting outputs from the mixers are low-pass filtered and digitized by analog-to-digital (A/D) converters to obtain the in-phase (I) and quadrature (Q) representative of the received vector.

Although the classical analog I/Q demodulator provides a clear example of how baseband conversion can be implemented, in most modern systems I/Q demodulation is performed *after* digitization. This has the advantage of avoiding so-called "I/Q mismatch" problems which hamper the analog implementation (Pun, Franca et al. 2003). The flipside of this, however, is that digital I/Q demodulators require a rate that is *twice* that of each of the A/D converters in Figure 7; in effect, complex sampling requires real sampling at twice the rate. Given the high sample rates obtainable with modern A/D converters, however, this is usually not a problem.

There are actually several techniques, referred to as "direct sampling digital coherent detection techniques" (Pun, Franca et al. 2003), for performing baseband conversion after digitization, which were developed in the early 1980s (Rice and Wu 1982; Waters and Jarrett 1982; Rader 1984). A detailed discussion of these techniques is beyond the scope of this thesis; we will simply use the result that the signal s_{IF} given by (2.9) can be obtained in baseband form.

2.1.4 Video signal

After quadrature sampling of the IF signal s_{IF}, a processor based on the fast Fourier transform (FFT) resolves the beat frequency spectrum into frequency and range bins. Following Stove (Stove 1992), we refer to the beat signal after frequency analysis as the *video signal*.

As explained in Section 2.1.3, the portion of the IF signal that is within the receiver bandwidth is a pulse train with pulse length $T - \tau$ and pulse repetition interval T. Since the IF signal is periodic with period T, its target range information can be obtained from the Fourier transform S_{IF} of a single pulse:

$$S_{IF}(f) = \int_{-\infty}^{\infty} s_{IF}(t) \exp(-j2\pi f t)\, dt, \qquad\qquad (2.13)$$

where $s_{IF}(t)$ is given by (2.9). Here and throughout this thesis, functions represented by uppercase letters are Fourier transforms of the functions represented by the corresponding lowercase letters.

Substituting (2.9) into (2.13), evaluating the Fourier integral, and taking its absolute value, we find

$$|S_{IF}(f)| = (T - \tau)\mathrm{sinc}[(T - \tau)(f - \alpha\tau)], \qquad\qquad (2.14)$$

where $\mathrm{sinc}(\cdot)$ is the normalized "sinc" function defined as

$$\mathrm{sinc}(x) \equiv \frac{\sin(\pi x)}{\pi x}.$$

An illustrative plot of the amplitude spectrum is shown in Figure 8. The target at range $R = c\tau/2$ shows up as a peak at the target beat frequency $f_b = \alpha\tau$. Although the spectrum is plotted as a function of frequency, the abscissa can be scaled by a factor $(cT/2B)$ to yield a plot of target reflectivity versus range; this plot is called the *range profile*.
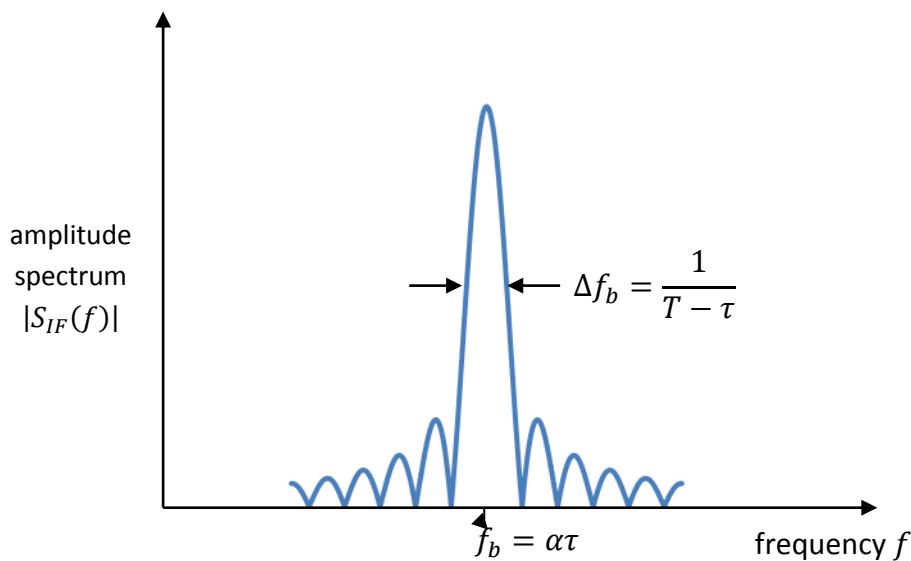
Figure 8 Amplitude spectrum $|S_{IF}(f)|$ of one pulse of the in-band portion of the IF signal. The spectrum as is a "sinc" shaped peak at the target beat frequency $f_b = \alpha\tau$, where α is the sweep rate and τ the two-way propagation delay. The width Δf_b of the peak (strictly, width at -3.9 dB) is the reciprocal of the duration of the pulse, $1/(T - \tau)$.

As stated in the Introduction, in practice the spectral analysis is performed by an analog-to-digital converter (ADC) followed by a processor based on the fast Fourier transform (FFT). Approximating the spectrum in this way involves a number of practical considerations:

- **Nyquist criterion**. Typically, the FMCW radar is only designed to detect targets up to a certain maximum range or *instrumented range* R_{max}. In order to prevent aliasing of the spectra of targets within R_{max}, the ADC sample rate f_s should be chosen at least twice the maximum beat frequency $f_{b,max}$:

$$f_s \geq 2f_{b,max}. \tag{2.15}$$

In order to prevent out-of-band noise from folding back into the target spectrum, the beat signal is typically passed through an *anti-aliasing filter*, which is a low-pass filter with a cutoff frequency between the maximum beat frequency $f_{b,max}$ and the Nyquist frequency $f_s/2$.

- **ADC interval.** As explained in Section 2.1.3, during the initial τ_{max} seconds of each sweep, a portion of the beat signal for targets within the instrumented range is outside the bandwidth of the ADC. This interval is usually omitted by delaying the sampling by τ_{max} seconds from the beginning of each sweep, or alternatively by setting the samples collected during the initial τ_{max} to zero {Adamski, 2000 #24}. As a result, the spectral width of a 'point' target is $\Delta f_b = 1/(T - \tau_{max})$ for all targets within the instrumented range.

- **Sidelobe apodization**. The beat signal spectrum $S_{IF}(f)$ given by (2.14) has the characteristic 'sinc' shape as predicted by Fourier theory. The range side lobes in this case are only 13.3 dB lower than the main lobe, which is not satisfactory as it can result in the occlusion of small nearby targets as well as introducing clutter from the adjacent lobes into the main lobes. To counter these undesirable effects, a *window function* (Harris 1978) is usually applied to the sampled IF signal prior to FFT frequency estimation. In our simulation in Chapter 0, we employ a Hamming window with a highest sidelobe level of -43 dB.

These practical aspects are of importance in explaining our simulation in Chapter 0[9].

To summarize, we have analyzed the generation and spectral analysis of the beat signal in mathematical detail for ideal, *linear* frequency sweeps. In the following section, we investigate how this process is affected if the sweeps are *nonlinear* – in particular, if they are perturbed by *sinusoidal* frequency sweep nonlinearity.

2.2   The effect of sinusoidal nonlinearity in the frequency sweep

This section presents an analysis describing the effects on the range resolution of homodyne linear FMCW radar of sinusoidal nonlinearities in the frequency sweep. Our discourse follows the analyses of Richter (Richter, Jensen et al. 1973), Griffiths (Griffiths 1991; Griffiths and Bradford 1992), and Piper (Piper 1995).

2.2.1   Analytical development

We treat the chirp signal as a nominally-linear FM sweep of rate α and unit amplitude, with the frequency error expressed in terms of a departure from frequency sweep linearity with amplitude δ_f and frequency f_{sl}:

$$f_{TX}(t) = f_c + \alpha t + \delta_f \cos(2\pi f_{sl} t), \qquad -\frac{T}{2} < t < \frac{T}{2}. \tag{2.16}$$

This non-linear time-frequency characteristic is illustrated together with its linear counterpart in Figure 9.

---

[9] As explained in 2.1.3.2, another important digital signal processing step is the digital I/Q demodulation. In our simulation in Chapter 0, we assume this has already been done, and used complex samples directly.
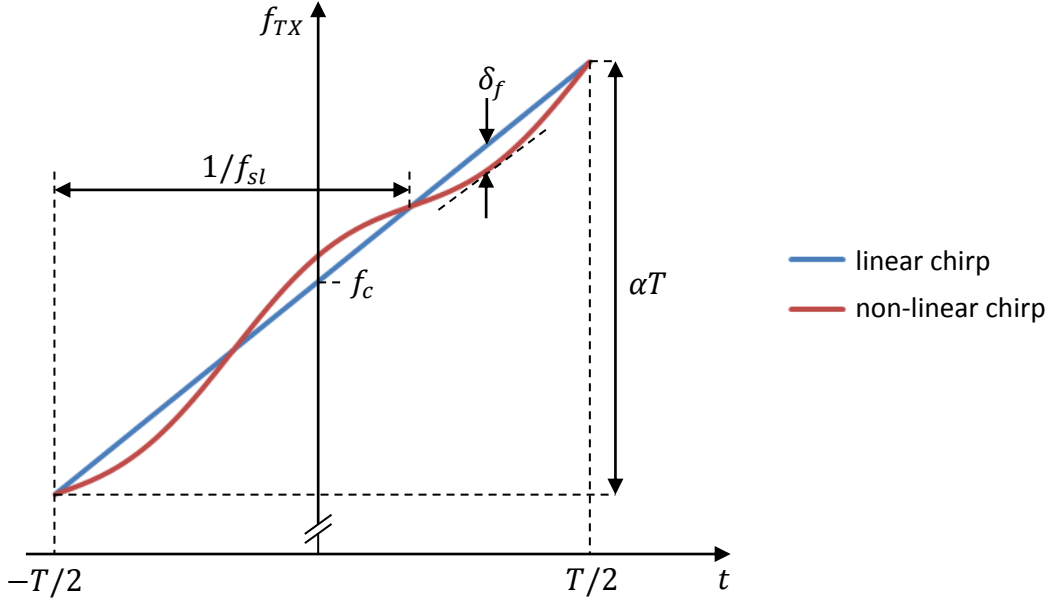
Figure 9 Time-frequency characteristics of a linear chirp (blue line) and a non-linear chirp (red curve). The linear chirp on the interval $[-T/2, T/2]$ has a center frequency f_c, duration T, chirp rate α, and frequency deviation (or 'bandwidth') $B = \alpha T$. The non-linear chirp is

The phase of the transmitted signal ϕ_{TX} is obtained by integrating the instantaneous *angular* frequency $\omega_{TX} = 2\pi f_{TX}$ in accordance with (2.4). Arbitrarily setting $\phi_{TX} = 0$ at $t = 0$ (there is no loss of generality here), we thus have the relation

$$\phi_{TX}(t) = 2\pi \int_0^t f_{TX}(t')\, dt'. \tag{2.17}$$

Inserting the expression (2.16) for f_{TX} into (2.17), we find

$$\phi_{TX}(t) = 2\pi \left(f_c t + \frac{1}{2}\alpha t^2 \right) + A_{sl} \sin(2\pi f_{sl} t), \tag{2.18}$$

where $A_{sl} = \delta_f / f_{sl}$ is the "modulation index" of the transmitted chirp, i.e., its maximum phase error.

The phase of the beat signal is given by (cf. (2.8))

$$\phi_{IF}(t) = \phi_{TX}(t) - \phi_{TX}(t - \tau), \tag{2.19}$$

where τ is the target transit time as defined by (2.6). Inserting (2.18) into (2.19) yields

$$\phi_{IF}(t) = 2\pi \left(f_c \tau + \alpha \tau t - \frac{1}{2}\alpha \tau^2 \right) + A_{sl}\left[\sin(2\pi f_{sl} t) - \sin\left(2\pi f_{sl}(t - \tau)\right) \right] \tag{2.20}$$

or, using trigonometric identities to factorize the IF phase error term,

$$\phi_{IF}(t) = 2\pi \left(f_c \tau + \alpha \tau t - \frac{1}{2}\alpha \tau^2 \right) + 2 A_{sl} \sin(\pi f_{sl} \tau) \cos\left[2\pi f_{sl}\left(t - \frac{\tau}{2} \right) \right]. \tag{2.21}$$

The baseband dechirped signal with envelope $r(t)$ is therefore given by (cf. (2.9)):

$$s_{IF}(t) = r(t)\exp[j\phi_{IF}(t)]$$
$$= r(t)\exp\left[j\left(\phi' + 2\pi\alpha\tau t + \beta\cos\left[2\pi f_{sl}\left(t - \frac{\tau}{2}\right)\right]\right)\right] \qquad (2.22)$$

where $\phi' = 2\pi(f_c\tau - \alpha\tau^2/2)$ is a constant phase term and

$$\beta \equiv 2A_{sl}\sin(\pi f_{sl}\tau) \qquad (2.23)$$

is the "modulation index", or maximum phase error, of the IF signal.

The expression (2.22) is recognizable from narrowband phase modulation theory. It can be expanded as

$$s_{IF}(t) = r(t)\exp[j(\phi' + 2\pi\alpha\tau t)]\left\{1 + j\beta\cos\left[2\pi f_{sl}\left(t - \frac{\tau}{2}\right)\right]\right.$$
$$\left. - \frac{1}{2!}\beta^2\cos^2\left[2\pi f_{sl}\left(t - \frac{\tau}{2}\right)\right] + \cdots\right\} \qquad (2.24)$$

Now, if we assume that the peak phase error is small, i.e.,

$$\beta \ll 1, \qquad (2.25)$$

then only the first two terms of the expansion in (2.24) are significant. Thus the baseband dechirped signal is approximately

$$s_{IF}(t) \approx r(t)\exp[j(\phi' + 2\pi\alpha\tau t)]\left\{1 + \frac{\beta}{2}\exp\left[j2\pi f_{sl}\left(t - \frac{\tau}{2}\right)\right] + \frac{\beta}{2}\exp\left[-j2\pi f_{sl}\left(t - \frac{\tau}{2}\right)\right]\right\} \quad (2.26)$$

which is the distortionless point-target response, plus a pair of sidelobes, or *paired echoes*, at $\pm f_{sl}$. The amplitude of each of these sidebands is $\beta/2$.

2.2.1.1 *Limit of long-wavelength phase errors*
For long-wavelength phase errors such that the sidelobe ripple period is much larger than the target transit time, i.e.,

$$\frac{1}{f_{sl}} \gg \tau, \qquad (2.27)$$

(2.23) is well approximated by

$$\beta \approx A_{sl}\omega_{sl}\tau, \qquad (2.28)$$

where $\omega_{sl} \equiv 2\pi f_{sl}$ is the angular ripple frequency. Thus, for long-wavelength phase errors, the modulation parameter β in the beat signal increases linearly with the target transit time τ, and hence with target range. Physically, we can say that for delays which are small compared to the wavelength of the phase error, the transmitted and received phase errors 'cancel out'[10].

---

[10] This is in contrast to conventional pulse compression radars, in which the 'paired echo' effect is independent of target range {Klauder, 1960 #20}. As a result, requirements on frequency sweep linearity can be considerably less stringent for FMCW radar than for LFM pulse compression radar, as noted by Griffiths {Griffiths, 1991 #36}.

2.2.1.2   General phase errors

In the preceding discussion, we considered a sinusoidal phase error. Here, we argue that the above analysis can be extended to general phase errors.

A general phase error can be written in the form

$$f_{TX}(t) = f_c + \alpha t + f_{\epsilon,TX}(t), \qquad -\frac{T}{2} < t < \frac{T}{2}. \tag{2.29}$$

The error frequency $f_{\epsilon,TX}(t)$ can be expanded as a Fourier series:

$$f_{\epsilon,TX}(t) = \frac{a_0}{2} + \sum_{n=1}^{\infty}\left[a_n \cos\left(\frac{2\pi n t}{T}\right) + b_n \sin\left(\frac{2\pi n t}{T}\right)\right]. \tag{2.30}$$

where

$$a_n = \frac{1}{\pi}\int_{-\pi}^{\pi} f_\epsilon\left(\frac{2\pi t}{T}\right)\cos(nx)\,dx, \qquad b_n = \frac{1}{\pi}\int_{-\pi}^{\pi} f_\epsilon\left(\frac{2\pi t}{T}\right)\sin(nx)\,dx. \tag{2.31}$$

Now, the constant term $a_0/2$ in (2.30) has only the effect of changing the center frequency $f_c\tau$ of the chirp, and since the center frequency is present in the beat signal phase only in the constant phase term $f_c\tau$, this term has no effect on the amplitude spectrum of the beat signal.

Thus, neglecting the constant frequency term $a_0/2$ and integrating (2.30), we find that the phase error $\phi_{\epsilon,TX}(t)$ is given by

$$\begin{aligned}\phi_{\epsilon,TX}(t) &= 2\pi \int_0^t f_\epsilon(t')\,dt' \\ &= \sum_{n=1}^{\infty}\left[\frac{a_n T}{n}\sin\left(\frac{2\pi n}{T}t\right) - \frac{b_n T}{n}\cos\left(\frac{2\pi n}{T}t\right)\right].\end{aligned} \tag{2.32}$$

(Here we have omitted a constant phase term which also has no effect on the range profile).

The phase error in the IF signal, $\phi_{\epsilon,IF}$, is the difference between the transmitted phase error $\phi_{\epsilon,TX}$ and its version delayed by τ:

$$\phi_{\epsilon,IF}(t) = \phi_{\epsilon,TX}(t) - \phi_{\epsilon,TX}(t - \tau). \tag{2.33}$$

Inserting (2.32) into (2.33), subtracting term by term, and applying trigonometric identities as before, we find

$$\phi_{\epsilon,IF}(t) = \sum_{n=1}^{\infty} 2\sin\left(\frac{\pi n}{T}\tau\right)\left[\frac{a_n T}{n}\cos\left(\frac{2\pi n}{T}\left(t - \frac{\tau}{2}\right)\right) + \frac{b_n T}{n}\sin\left(\frac{2\pi n}{T}\left(t - \frac{\tau}{2}\right)\right)\right]. \tag{2.34}$$

Now, a little thought shows that if we substitute (2.34) for the single-tone phase error $\beta\cos\left(2\pi f_{sl}(t - \tau/2)\right)$ in (2.22) and expand the factor $\exp\left(j\phi_{\epsilon,IF}\right)$ as a Taylor series, then the higher-order terms can be neglected as long as $\phi_{\epsilon,IF}$ is small compared to unity. A sufficient condition for this is that the amplitudes of the frequency errors are much smaller than the sweep repetition frequency, i.e.,

$$a_n \ll \frac{1}{T} \quad \text{and} \quad b_n \ll \frac{1}{T}. \tag{2.35}$$

In this case, the target beat spectrum consists of a superposition of 'paired echoes' spaced at multiples of the sweep repetition frequency, $1/T$, from the desired target beat signal.

In short, within small-angle approximations for the phase error, the 'paired echoes' associated with the harmonics of the phase error merely superpose. Hence, an algorithm that compensates the 'paired echoes' for a chirp perturbed by sinusoidal phase errors and is *linear* should also work for general phase errors, provided that these errors are sufficiently small. The derivation of such phase error compensation algorithm is the subject of the next chapter.

3 An algorithm for compensating the effect of phase errors on the FMCW beat signal spectrum

In this chapter, we present a novel algorithm for compensating the effect of phase errors on the FMCW beat signal spectrum by digital post-processing of the beat signal. Given amount of effort that is currently put into making chirps linear, the existence of this algorithm is a very significant in the field of FMCW ranging, and could render such elaborate chirp linearization methods obsolete.

This chapter is organized in three sections. In Section 3.1, we discuss similar algorithms that were devised by others, and highlight the differences with our approach. In Section 3.2, we establish some mathematical preliminaries – namely the quadratic phase filter and the Fresnel transform – which will allow us to describe the algorithm more succinctly. In Section 3.3, we present a flow chart describing the algorithm. In Section 3.4, we present an analytical derivation of the algorithm for temporally infinite chirps, and show that the algorithm is exact in this case. In Section 3.5, we apply the algorithm to finite chirps, and show that it remains approximately valid for chirps with large time-bandwidth product and for which the phase error function contains only low frequencies.

3.1 Prior work

A signal processing method was devised, apparently independently, by Burgos-Garcia et al. (Burgos-Garcia, Castillo et al. 2003) and Meta et al. (Meta, Hoogeboom et al. 2006; Meta, Hoogeboom et al. 2007) to compensate for non-linearities in the frequency sweep (or equivalently, phase errors in the phase) of FMCW signals. (Actually, the system described in (Burgos-Garcia, Castillo et al. 2003) is a *heterodyne* time-domain pulse compression radar instead of a *homodyne* FMCW radar, but the results can be applied to the latter case). The algorithm, which operates directly on deramped data, corrects non-linearity effects for the whole range at once, and is computationally efficient.

Burgos-Garcia et al. and Meta et al. present the algorithm in a slightly different form, which is also different from the one described here. In particular (as we will explain in more detail in Section 3.4),

1. In the last step of the algorithm described by Burgos-Garcia et al. (Burgos-Garcia, Castillo et al. 2003), the phase error function in the receive signal, which they call $\phi_{EX}(t)$, is used directly to cancel the residual phase error after removal of the transmitted errors and range deskew. This is based on their stated assumption that the beat signal from the ith target is a narrowband signal centered at the frequency $f_i = \alpha\tau_i$. Our derivation shows that this assumption is not necessary, and that a skew-filtered version of the phase error function can be used in the case that the beat signal is not narrowband[11].

2. The algorithm described by Meta (Meta, Hoogeboom et al. 2006) does use a filtered version of the phase error function in the last step. However, this version is a Fresnel transform of the phase error function, whereas we believe it should be an *inverse* Fresnel transform[12].

---

[11] The author initiated a private e-mail correspondence with Mr. Burgos-Garcia, but unfortunately he was not at liberty to discuss the details of the algorithm under the terms of his project contract with the Spanish defense company Indra EWS.

[12] The author also e-mailed Mr. Meta about this, but unfortunately he was too busy to study the derivation. Interestingly, an international an international patent application was submitted for this technique (Meta 2007), but at the time of writing is deemed to be withdrawn.

Moreover, (Burgos-Garcia, Castillo et al. 2003) and (Meta, Hoogeboom et al. 2006) use heuristic arguments to justify the steps, and no formal proof of the algorithm was given. Our analytical derivation in Section 3.4 is thus a novel contribution to the literature on this subject.

3.2 Mathematical preliminaries

The key component of the phase error compensation (PEC) algorithm to be described is the quadratic phase filter (QPF). As a prelude to our presentation of the algorithm, here we first discuss the properties of this filter, as well as an integral transform called the *Fresnel transform* associated with it (Gori 1994; Papoulis 1994).

3.2.1 The quadratic phase filter

A QPF is an all-pass system with quadratic phase. We denote by $q_\alpha(t)$ its impulse response and by $Q_\alpha(f)$ its transfer function:

$$q_\alpha(t) = \sqrt{-j\alpha} \, \exp(j\pi\alpha t^2) \leftrightarrow Q_\alpha(f) = \exp\left(-j\pi \frac{f^2}{\alpha}\right). \tag{3.1}$$

where the double arrow ($\leftrightarrow$) denotes a Fourier transform pair, and the time and frequency domains are identified by the arguments t and f, respectively. Note that since neither $q_\alpha(t)$ nor $Q_\alpha(f)$ is square-integrable, this Fourier transform pair should be interpreted in the generalized sense as the limit as $\sigma \to 0^+$ of the Fourier transform of the *complex Gaussian beam* $\exp(-\pi(\sigma - j\alpha)t^2)$, where σ and α are real parameters (Papoulis 1977).

The QPF is a dispersive filter which introduces a *group delay* proportional to the frequency. Group delay is a measure of the time delay of the amplitude envelope of a sinusoidal component; it is in general different from the *phase delay*, which is the time delay of the phase. The group delay of a constant-modulus filter $H(f) = \exp[j\Phi(f)]$ is given by

$$t_g(f) = -\frac{1}{2\pi} \frac{d\Phi}{df}. \tag{3.2}$$

Thus, the group delay $t_{g,\alpha}(f)$ of the QPF given by (3.1) is

$$t_{g,\alpha}(f) = \frac{f}{\alpha}. \tag{3.3}$$

Hence, the group delay of a QPF is linearly proportional to the frequency. (Incidentally, the group delay of a QPF is the inverse function of the instantaneous frequency of its impulse response: $f_{i,\alpha}(t) = \alpha t$. This result does not hold in general, but holds here because $q_\alpha(t)$ is a so-called 'asymptotic' signal (Boashash 1992)).

3.2.2 The Fresnel transform

The Fresnel transform with chirp parameter α of a function $s(t)$, denoted $s_\alpha(t)$ here, is by definition the output of a QPF with input $s(t)$:

$$s_\alpha(t) = \sqrt{-j\alpha} \int_{-\infty}^{\infty} s(t') \exp[j\pi\alpha(t - t')^2] \, dt' = s(t) * q_\alpha(t), \tag{3.4}$$

where the asterisk ($*$) denotes the convolution product. The inversion formula reads

$$s(t) = \sqrt{j\alpha} \int_{-\infty}^{\infty} s_\alpha(t) \exp[-j\pi\alpha(t-t')^2]\, dt' = s_\alpha(t) * q_{-\alpha}(t), \tag{3.5}$$

so that the inverse transform simply equals the Fresnel transform with parameter $-\alpha$.

Let us denote by $S(f)$ the Fourier transform of a function $s(t)$. From the definition (3.4) and the convolution theorem, it follows that the Fourier transform $S_\alpha(f)$ of $s_\alpha(t)$ equals

$$S_\alpha(f) = S(f) \exp\left(-j\pi\frac{f^2}{\alpha}\right). \tag{3.6}$$

It is also useful to investigate an asymptotic limit of the Fresnel transform. Based on the limit (Papoulis 1977)

$$\lim_{\alpha\to\infty} \sqrt{-j\alpha}\, \exp(j\pi\alpha t^2) = \delta(t), \tag{3.7}$$

where $\delta(\cdot)$ denotes the Dirac delta function, it follows that in the limit $\alpha \to \infty$ the Fresnel transform of a function approaches the function itself, i.e.,

$$\lim_{\alpha\to\infty} s_\alpha(t) = s(t). \tag{3.8}$$

The Fresnel transform manifests itself several areas of signal and image processing, including pulse compression, fiber-cable communications and dispersion, and Fresnel diffraction and optical filtering (Papoulis 1994). Here, it will allow us to give a concise description of the PEC algorithm.

3.3 Description of the phase error compensation algorithm

Suppose the transmitted signal is perturbed by a phase error $2\pi\epsilon(t)$. We assume that $\epsilon(t)$ is known (its estimation is discussed in Chapter 0), and define the *phase error function*

$$s_\epsilon(t) \equiv \exp[j2\pi\epsilon(t)]. \tag{3.9}$$

The correction algorithm, shown schematically in Figure 10, consists of the following three steps:

1. The complex-valued deramped data $s_{IF}(t)$ is first multiplied by the complex conjugate of the phase error function, $s_\epsilon^*(t)$, in order to eliminate phase errors resulting from transmitted non-linearities.
2. The resulting signal, $s_{IF2}(t)$, is then passed through a *deskew filter*[13] with frequency response

$$Q_{-\alpha}(f) = \exp\left(j\pi\frac{f^2}{\alpha}\right), \tag{3.10}$$

where α is the (nominal) chirp rate of the transmitted chirp. Thus, the deskew filter is a QPF with a parameter a negative group delay $-f/\alpha$, which has the effect of aligning the received

---

[13] Incidentally, the deskew filter is commonly used in synthetic aperture radar (SAR) signal processing, where its purpose is to remove the range-dependent phase term $-\pi\alpha\tau^2$ from the beat signal (cf. Section 2.1.3) of relevance in SAR applications. Since this phase term is called the residual video phase (RVP), the filter is also called an 'RVP filter' (Carrara, Goodman et al. 1995) in this context.

non-linearities in time[14]. (In the parlance of Section 3.2.2, s_{IF3} is the inverse Fresnel transform of s_{IF2}).

3. Finally, the deskewed signal $s_{IF3}(t)$ is multiplied by the Fresnel transform $s_{\epsilon,\alpha}(t)$ of the phase error function $s_{\epsilon}(t)$. convolution product $s_{\epsilon,\alpha}(t)$ of the phase error function $s_{\epsilon}(t)$ with a *skew filter* with an impulse response $q_{\alpha}(t)$, the frequency response $Q_{\alpha}(f)$ of which corresponds to the one in (3.10) with the sign of α reversed.

The last step removes the received non-linearities to obtain the compensated signal $s_{IF4}(t)$.
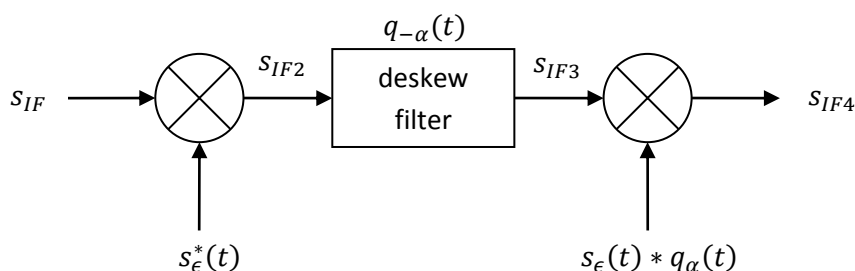
Figure 10 Schematic diagram of the phase error compensation algorithm. In the first step, the intermediate frequency (IF) signal $s_{IF}(t)$ is multiplied by the complex conjugate of the phase error function, $s_{\epsilon}^{*}(t)$, to the remove the transmitted phase errors. The resulting signal $s_{IF2}(t)$ is inverse Fresnel transformed by passing it through a *deskew filter* with impulse response $q_{-\alpha}(t)$. This results in a signal $s_{IF3}(t)$ in which the remaining phase errors, which emanate from the received signal, are aligned in time. Finally, $s_{IF3}(t)$ is multiplied by a the Fresnel transform of the phase error function, $s_{\epsilon}(t) * q_{\alpha}(t)$, to obtain the corrected IF signal s_{IF4}.

As an example to visualize the operation of the PEC algorithm in the time-frequency domain, Figure 11 shows (upper figure) a transmitted linear FMCW signal which is perturbed by triangle-shaped frequency sweep non-linearity and two received echoes of this signal. The non-linearities in the transmit chirp signal result in nonlinearities in the beat signal (lower figure), which are the difference between the transmitted and received non-linearities. As explained in Chapter 1, the non-linearities in the beat signal deteriorate the range resolution because they spread the target energy through different frequencies. This effect generally increases at greater range, when the transmitted and received signals are less correlated.

---

[14] We will refer to the phase errors remaining after the range deskew step as 'residual' phase errors.
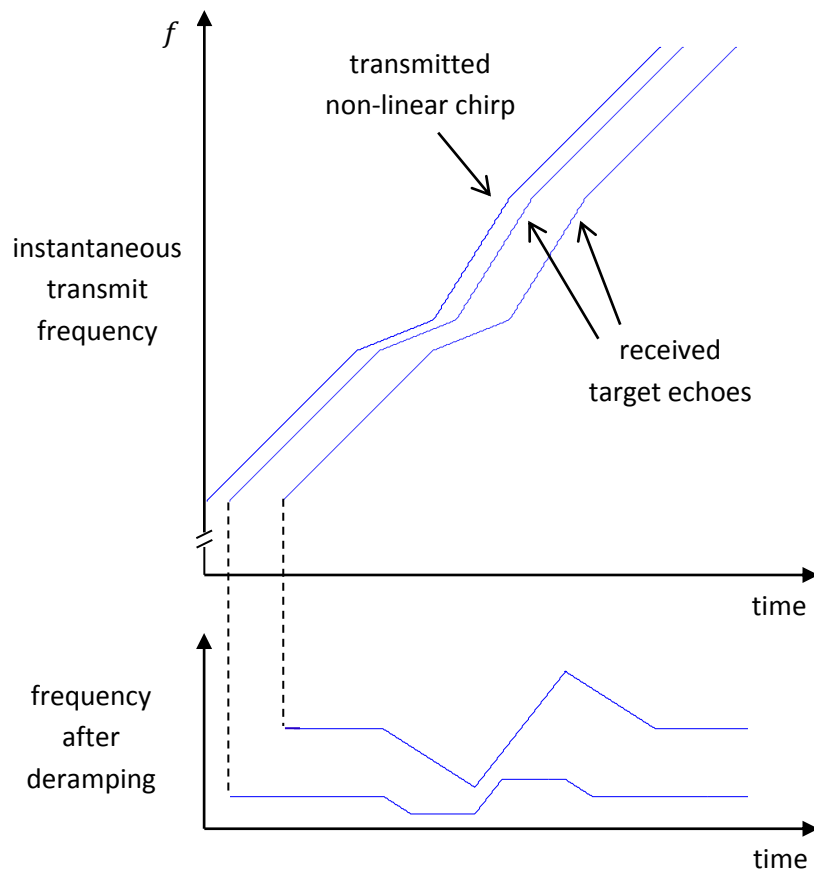
Figure 11 Deramping of FMCW signals. The upper figure shows the instantaneous frequency of the transmitted chirp (solid line) and two received echoes (dashed lines). The lower figure depicts the corresponding two beat signals. The resulting frequencies of the beat signals are not constant, and their shape varies with target distance. The spreading of the beat signal in frequency is greater for the target response at larger distance than at the closer. (After (Meta, Hoogeboom et al. 2006)).

Figure 12 shows a block diagram of the PEC algorithm. The collected non-linear deramped data, s_{IF}, is multiplied by $s_\epsilon^*(t)$
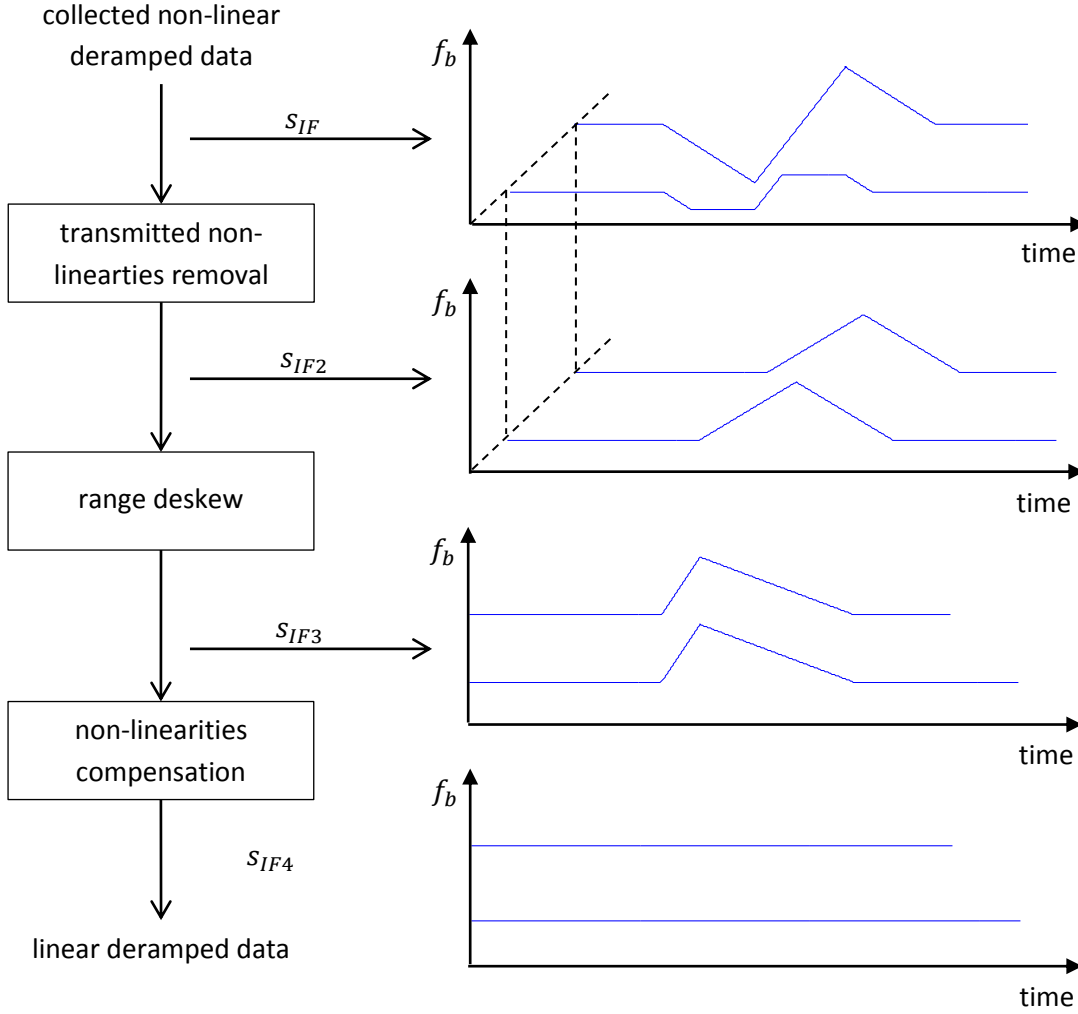
Figure 12 Block diagram of the phase error compensation algorithm. The diagrams on the right represent the instantaneous frequency of the beat signal, $f_b(t)$, at successive steps of the algorithm. (After (Meta, Hoogeboom et al. 2006)).

In short, by performing a multiplication, a convolution, and another multiplication on the deramped data, the effect of phase errors in the transmit signal can be removed, assuming the form of these errors is known. In the following section, we explain these steps analytically.

3.4   Derivation of the algorithm for temporally infinite chirps

In this section, we present an analytical derivation of the phase error compensation algorithm for temporally infinite chirps. We show that the compensation algorithm is exact in this case.

3.4.1   Recapitulation of the FMCW principle for linear chirps

For the purpose of comparison and for future reference, we first reiterate the principle of FMCW range measurement for the case in which the transmitted signal is a temporally infinite *linear* chirp, unperturbed by any phase error. The transmit signal in this case can be represented as the real part of

$$s_{TX,lin}(t) = \exp\left[j2\pi\left(f_c t + \frac{1}{2}\alpha t^2\right)\right],$$ (3.11)

where f_c is the carrier frequency, t is the time variable, and α is the frequency sweep rate. Note that in contrast to Eq. (2.2), there is no envelope factor $\text{rect}(t/T)$ in (3.11) since we are assuming that the transmitted chirp is temporally infinite.

The received signal is a delayed version of the transmitted one (amplitude variations are not considered in this derivation):

$$s_{RX,lin}(t) = \exp\left[j2\pi\left(f_c(t-\tau) + \frac{1}{2}\alpha(t-\tau)^2\right)\right], \tag{3.12}$$

where τ is the round-trip time delay. In homodyne FMCW radar, the transmitted and received signals are then mixed to generate the beat signal:

$$\begin{aligned} s_{IF,lin}(t) &= s_{Tx,lin}(t)s_{Rx,lin}^*(t) \\ &= \exp\left[j2\pi\left(f_c\tau + \alpha\tau t - \frac{1}{2}\alpha\tau^2\right)\right]. \end{aligned} \tag{3.13}$$

The beat signal is a sinusoidal signal with a frequency $\alpha\tau$ proportional to the round-trip time delay τ, and hence to the target range. The frequency information can be extracted using a Fourier transform.

More precisely, except for a constant phase term, the Fourier transform $S_{IF,lin}(f)$ of $s_{IF,lin}(t)$ is a Dirac delta function centered at the beat frequency $\alpha\tau$:

$$S_{IF,lin}(f) = \exp\left[j2\pi\left(f_c\tau - \frac{1}{2}\alpha\tau^2\right)\right]\delta(f - \alpha\tau). \tag{3.14}$$

Of course in practice, the beat signal is observed over a finite interval, and the ideal response (3.14) is convolved with the Fourier transform of the window function used.

3.4.2 Introduction of phase errors

When frequency nonlinearities are present in the transmitted signal, the signal modulation is no longer an ideal chirp; the phase of the signal can be described as an ideal chirp plus a non-linear error function $\epsilon(t)$:

$$\begin{aligned} s_{TX}(t) &= \exp\left[j2\pi\left(f_ct + \frac{1}{2}\alpha t^2 + \epsilon(t)\right)\right] \\ &= s_{TX,lin}(t)s_\epsilon(t). \end{aligned} \tag{3.15}$$

The last term, accounting for systematic non-linearity of the frequency modulation, limits the performance of conventional FMCW sensors. This phase term increases spectral bandwidth, resulting in range resolution degradation and losses in terms of signal-to-noise ratio.

The beat signal is now represented by

$$\begin{aligned} s_{IF}(t) &= \exp\left[j2\pi\left(f_c\tau + \alpha\tau t - \frac{1}{2}\alpha\tau^2 + \epsilon(t) - \epsilon(t-\tau)\right)\right] \\ &= s_{IF,lin}(t)s_\epsilon(t)s_\epsilon^*(t-\tau). \end{aligned} \tag{3.16}$$

Equation (3.16) differs from (3.11) for the present of the last term $(\epsilon(t) - \epsilon(t-\tau))$.

3.4.3 First step: removal of phase errors emanating from the transmitted signal

Assuming the non-linearity function $s_\epsilon(t)$ is known (its estimation is discussed in Chapter 0), the range-independent effect of the non-linear term in the beat frequency can be removed by the following multiplication:

$$
\begin{aligned}
s_{IF2}(t) &= s_{IF}(t)s_\epsilon^*(t) \\
&= \exp\left[j2\pi\left(f_c\tau + \alpha\tau t - \frac{1}{2}\alpha\tau^2 - \epsilon(t-\tau)\right)\right].
\end{aligned}
\tag{3.17}
$$

The multiplication – which can because we have assumed that we have complex samples (both I and Q components) of the beat signal – removes the nonlinearities in the beat signal induced by the nonlinear part of the transmitted signal. The residual nonlinearity term is present now only as a result of the received signal. In order to remove this nonlinearity term with a single reference function, any dependence on the time delay must be eliminated.

3.4.4 Second step: range deskew

To this end, the signal s_{IF2} is passed through a quadratic phase filter $q_{-\alpha}(t)$ with chirp parameter $-\alpha$, where α is the nominal chirp rate of the transmitted sweep; that is, s_{IF2} is *inverse Fresnel transformed* (or in the parlance of SAR signal processing, *deskew-filtered*) to obtain a signal s_{IF3}:

$$
s_{IF3}(t) = s_{IF2}(t) * q_{-\alpha}(t)
\tag{3.18}
$$

It will be shown that this convolution has the effect of aligning in time the phase errors emanating from the received signal. This result can be derive d both in the frequency domain and in the time domain. As an internal check on our results, we have done both, and present the derivations below.

3.4.4.1 Frequency-domain approach

In this approach, we determine the spectrum $S_{IF3}(f)$ of the signal $s_{IF3}(t)$ given by (3.18). Taking the Fourier transform of (3.18), we obtain, by the convolution theorem and the definition of the deskew filter transfer function (3.10),

$$
\begin{aligned}
S_{IF3}(f) &= S_{IF2}(f)Q_{-\alpha}(f) \\
&= S_{IF2}(f)\exp\left(j\pi\frac{f^2}{\alpha}\right).
\end{aligned}
\tag{3.19}
$$

To evaluate $S_{IF2}(f)$, we depart from the following expression for $s_{IF2}(t)$ (which is easily seen by comparison of (3.16) and (3.17)):

$$
s_{IF2}(t) = s_{IF,lin}(t)s_\epsilon^*(t-\tau).
\tag{3.20}
$$

Applying the convolution theorem to (3.20) yields

$$
S_{IF2}(f) = S_{IF,lin}(f) * \mathcal{F}\{s_\epsilon^*(t-\tau)\}(f),
\tag{3.21}
$$

where $\mathcal{F}\{\cdot\}(f)$ denotes the Fourier transform with frequency variable f. The first term, $S_{IF,lin}(f)$, is a Dirac delta function centered at the target beat frequency $\alpha\tau$, as was shown in Eq. (3.14). The second term can be expressed as

$$
\mathcal{F}\{s_\epsilon^*(t-\tau)\}(f) = \exp(-j2\pi f\tau)\, S_\epsilon^*(-f),
\tag{3.22}
$$

where $S_\epsilon(f)$ is the Fourier transform of the error signal $s_\epsilon(t)$. Inserting (3.14) and (3.22) into (3.21) yields

$$S_{IF2}(f) = \left\{ \exp\left[j2\pi \left(f_c\tau - \frac{1}{2}\alpha\tau^2 \right) \right] \delta(f - \alpha\tau) \right\} * \left\{ \exp(-j2\pi f\tau) S_\epsilon^*(-f) \right\}. \qquad (3.23)$$

Since convolution with $\delta(f - \alpha\tau)$ shifts the spectrum $\alpha\tau$ to the right, but leaves it otherwise unchanged, we have

$$S_{IF2}(f) = \exp\left[j2\pi \left(f_c\tau - \frac{1}{2}\alpha\tau^2 \right) \right] \exp[-j2\pi(f - \alpha\tau)\tau] S_\epsilon^*[-(f - \alpha\tau)] \qquad (3.24)$$

or, simplifying,

$$S_{IF2}(f) = \exp(j2\pi f_c\tau) \exp\left[j\frac{\pi}{\alpha}(-2f\alpha\tau + \alpha^2\tau^2) \right] S_\epsilon^*[-(f - \alpha\tau)], \qquad (3.25)$$

where we have arranged the argument of the second complex exponential as an "incomplete square".

Inserting (3.25) into (3.19), and thus multiplying $S_{IF2}(f)$ with the deskew filter transfer function $\exp(j\pi f^2/\alpha)$, now "completes the square" in this complex exponential. We obtain

$$S_{IF3}(f) = \exp(j2\pi f_c\tau) \exp\left[j\frac{\pi}{\alpha}(f - \alpha\tau)^2 \right] S_\epsilon^*[-(f - \alpha\tau)]. \qquad (3.26)$$

Since the right hand side of (3.26) depends on the frequency f through $f - \alpha\tau$ only, we can now use the sifting property of the Dirac delta function "in reverse" to express $S_{IF3}(f)$ as a convolution product:

$$S_{IF3}(f) = \left\{ \exp(j2\pi f_c\tau) \delta(f - \alpha\tau) \right\} * \left\{ \exp\left(j\frac{\pi}{\alpha} f^2 \right) S_\epsilon^*(-f) \right\}. \qquad (3.27)$$

This expression is similar to the one for S_{IF2}, Eq. (3.23), with one important difference: the second factor of the convolution product no longer depends on the target transit time τ.

By the convolution theorem, the inverse Fourier transform of $S_{IF3}(f)$, $s_{IF3}(t)$, is given by

$$s_{IF3}(t) = \mathcal{F}^{-1}\{\exp(j2\pi f_c\tau) \delta(f - \alpha\tau)\}(t) \cdot \mathcal{F}^{-1}\left\{ \exp\left(j\frac{\pi}{\alpha} f^2 \right) S_\epsilon^*(-f) \right\}(t), \qquad (3.28)$$

where $\mathcal{F}^{-1}\{\cdot\}(t)$ denotes the inverse Fourier transform with time variable t and the bullet ($\cdot$) denotes ordinary multiplication. The first term is a pure sinusoid with frequency $\alpha\tau$:

$$\mathcal{F}^{-1}\{\exp(j2\pi f_c\tau) \delta(f - \alpha\tau)\}(t) = \exp[j2\pi(f_c\tau + \alpha\tau t)]. \qquad (3.29)$$

The second term in (3.28) represents the residual phase error after range deskew. Since $S_\epsilon^*(-f)$ is the Fourier transform of $s_\epsilon^*(t)$, this term can, using (3.6), immediately be seen to be the inverse Fresnel transform of the complex conjugate of the error function s_ϵ, i.e.,

$$\begin{aligned}
\mathcal{F}^{-1}\left\{ \exp\left(j\frac{\pi}{\alpha} f^2 \right) S_\epsilon^*(-f) \right\}(t) &= s_\epsilon^*(t) * q_{-\alpha}(t) \\
&= [s_\epsilon(t) * q_\alpha(t)]^* \\
&= s_{\epsilon,\alpha}^*(t),
\end{aligned} \qquad (3.30)$$

where the second lines follows from the identity $q_{-\alpha}(t) = q_{\alpha}^*(t)$. Hence, the residual phase error function $s_{\epsilon,\alpha}^*$ is the complex conjugate of the Fresnel transform of the error function s_ϵ.

Inserting (3.29) and (3.30) into (3.28), we find

$$s_{IF3}(t) = \exp[j2\pi(f_c\tau + \alpha\tau t)]\, s_{\epsilon,\alpha}^*(t). \tag{3.31}$$

Thus, after range deskew, the beat signal is an ideal sinusoid with frequency $\alpha\tau$ perturbed by a phase error term $s_{\epsilon,\alpha}^*(t)$ which is independent of the target transit time τ.

3.4.4.2   *Time-domain approach*

The same result (3.31) can also be derived by a time-domain approach. Taking (3.18) as our starting point and inserting the definition (3.1) of $q_{-\alpha}$ in the convolution integral, we find

$$
\begin{aligned}
s_{IF3}(t) &= s_{IF2}(t) * q_{-\alpha}(t) \\
&= \int_{-\infty}^{\infty} \exp\left[j2\pi\left(f_c\tau - \frac{1}{2}\alpha\tau^2 + \alpha\tau u - \epsilon(u-\tau)\right)\right]\sqrt{j\alpha}\,\exp[-j\pi\alpha(t-u)^2]\,du.
\end{aligned}
\tag{3.32}
$$

By "completing the square" in the arguments of the complex exponentials, (3.32) can be written as

$$s_{IF3}(t) = \exp[j2\pi(f_c\tau + \alpha\tau t)]\sqrt{j\alpha}\int_{-\infty}^{\infty}\exp[-j\pi\alpha(u-\tau-t)^2]\,s_{\epsilon}^*(u-\tau)du, \tag{3.33}$$

or, performing the substitution $v = u - \tau$ and some manipulations,

$$
\begin{aligned}
s_{IF3}(t) &= \exp[j2\pi(f_c\tau + \alpha\tau t)]\sqrt{j\alpha}\int_{-\infty}^{\infty}\exp[-j\pi\alpha(t-v)^2]\,s_{\epsilon}^*(v)dv \\
&= \exp[j2\pi(f_c\tau + \alpha\tau t)]\left(\sqrt{-j\alpha}\int_{-\infty}^{\infty}\exp[j\pi\alpha(t-v)^2]\,s_{\epsilon}(v)dv\right)^* \\
&\equiv \exp[j2\pi(f_c\tau + \alpha\tau t)]\,s_{\epsilon,\alpha}^*(t),
\end{aligned}
\tag{3.34}
$$

where $s_{\epsilon,\alpha}(t)$ is the Fresnel transform of the error signal $s_\epsilon(t)$, in accordance with the definition (3.4). This reproduces our result (3.31) obtained by the frequency-domain approach.

3.4.5   Third step: removal of residual phase errors

The last step of the phase error compensation is now clear: multiply by s_{IF3} by $s_{\epsilon,\alpha}$ to remove the residual phase errors:

$$
\begin{aligned}
s_{IF4}(t) &= s_{IF3}(t)s_{\epsilon,\alpha}(t) \\
&= \exp[j2\pi(f_c\tau + \alpha\tau t)].
\end{aligned}
\tag{3.35}
$$

No error terms remain in the final, processed output, in which the residual video phase term $-\pi\alpha\tau^2$ has also been removed. Therefore, spectral analysis of $s_{IF4}(t)$ will yield the ideal target response.

To summarize, we have shown that if a temporally infinite chirp is perturbed by a general phase error term $s_\epsilon(t) = \exp[j2\pi\epsilon(t)]$, then its corresponding IF signal $s_{IF}(t)$ can be converted into an ideal response $s_{IF4}(t)$ by three steps: removal of the transmitted phase errors by multiplication with $s_\epsilon^*(t)$, range deskew by convolution with a quadratic phase filter $q_{-\alpha}(t)$, and finally, removal of the residual phase errors by multiplication with $s_{\epsilon,\alpha}(t) = s_\epsilon(t) * q_\alpha(t)$.

3.4.6 Comparison with Meta's algorithm

At this point, we note that our Equation (3.30) differs from the result obtained by Meta in his Equation (10) of (Meta, Hoogeboom et al. 2006) by the presence of a minus sign in the complex exponential. In other words, Meta uses an *inverse* Fresnel transform of the error function to obtain the correction factor for the residual phase errors, whereas our formulation uses the Fresnel transform[15]. As mentioned earlier, in a private correspondence with Mr. Meta he wrote that he unfortunately did not have time to look into this discrepancy, but acknowledge that one of his papers did contain a sign error. (This may, however, refer to the sign of the residual video phase in equation (3) of (Meta, Hoogeboom et al. 2006), which also contains a sign error).

The author believes that the method described by Meta contains an error or typo, and that the algorithm described in this thesis is correct. The fact that the two approaches – in the time and frequency domain – to the derivation of the algorithm lead to the same result corroborates this statement.

3.4.7 Narrowband IF signals: comparison with Burgos-Garcia's algorithm

In the algorithm described by Burgos-Garcia et al. (Burgos-Garcia, Castillo et al. 2003), the phase error $s_\epsilon(t)$ itself is used for the removal of the residual phase errors in the last step, instead of its Fresnel transform. This is based on their stated assumption that the IF signal is a narrowband signal, which is equivalent to saying that the error signal spectrum $S_\epsilon(f)$ contains only low frequencies.

Here, we verify that our algorithm reduces to Burgos-Garcia's algorithm in this case. Specifically, we will show that if $S_\epsilon(f)$ contains only low frequencies, then

$$s_{\epsilon,\alpha}(t) \approx s_\epsilon(t). \tag{3.36}$$

That is, the Fresnel transform of the error function is approximately equal to the error function itself, in which case our correction function for obtaining s_{IF4} from s_{IF3} reduces to the one given by Burgos-Garcia et al. (Burgos-Garcia, Castillo et al. 2003). We will also derive a quantitative criterion for the validity of (3.36).

To prove this statement, we adopt a frequency-domain approach. The Fourier transform $S_{\epsilon,\alpha}(f)$ of $s_{\epsilon,\alpha}(t)$ is given by (cf. (3.1))

$$\begin{aligned} S_{\epsilon,\alpha}(f) &= S_\epsilon(f) Q_\alpha(f) \\ &= S_\epsilon(f) \exp\left(-j\pi \frac{f^2}{\alpha}\right). \end{aligned} \tag{3.37}$$

Expanding $Q_\alpha(f)$ as a Taylor series, we obtain

$$S_{\epsilon,\alpha}(f) = S_\epsilon(f) \left[1 - j\pi \frac{f^2}{\alpha} + \frac{\pi^2}{2} \frac{f^4}{\alpha^2} - \cdots \right]. \tag{3.38}$$

---

[15] Note that whether the Fresnel transform or its inverse is applied at a certain stage depends on how we define the phase of the IF signal. If we choose $\phi_{IF} \equiv \phi_{TX} - \phi_{RX}$ as we have here, then for positive transmitted chirps we obtain positive beat signals. However, we could have just as well chosen to define $\phi_{RX} - \phi_{TX}$ as the phase of the IF signal, in which case Fresnel transforms would be replaced by inverse Fresnel transforms and vice versa. In either case, however, two *different* Fresnel transforms would be used in the algorithm, whereas Meta uses Fresnel transforms of the same sign for both steps.

The Fresnel transform of the error function, $s_{\epsilon,\alpha}(t)$ is obtained by taking the inverse Fourier transform of (3.38). The resulting series is called the *moment expansion* of the convolution product $s_{\epsilon,\alpha} = s_\epsilon * q_\alpha$ (Papoulis 1977).

Now, the first term in (3.38) inverse Fourier transforms to $s_\epsilon(t)$, which leads to the desired result (3.36). Further, it can be seen that in order for the higher-order terms to have negligible contributions, $S(f)$ must be bandlimited and its maximum frequency component f_{max} must be much smaller than $\sqrt{\alpha}$, i.e.,

$$f_{max} \ll \sqrt{\alpha}. \tag{3.39}$$

If (3.39), then the higher-order terms in the square bracket expression of (3.38) will be much smaller than unity will also increase with increasing order, so that only the zero-order term needs to be maintained. Thus, if approximation (3.39) is satisfied, then our algorithm reduces to the one described by Burgos-Garcia et al. (Burgos-Garcia, Castillo et al. 2003).

3.5 Application of the algorithm to finite chirps

In the previous section, we derived the PEC algorithm for general phase errors $\epsilon(t)$ and temporally *infinite* chirps, and showed that it was exact in this case. The purpose of this section is to apply the algorithm to *finite* chirps.

Actually, there are two varieties of the algorithm. One, discussed first in Section 3.5.1, is based on the algorithm for narrowband IF signals discussed in Section 3.4.7. It is shown that this 'narrowband algorithm' carries over directly to finite chirps provided the time-bandwidth product of the chirps is large (i.e., $BT \gg 1$). The second variety of the algorithm holds for wideband IF signals, and is the analog of the algorithm described and proved in Sections 3.4.1-3.4.6, and is described in Section 3.5.2. For the purpose of simplicity, we consider only *sinusoidal* phase errors (or, equivalently, sinusoidal frequency sweep non-linearity).

	infinite chirps	finite chirps
wideband IF	Sections 3.4.1-3.4.6	Section 3.5.1
narrowband IF	Section 3.4.7	Section 3.5.2

Table 2 Sections in which different varieties of the compensation algorithm are discussed. Of course, the compensation algorithms for finite chirps are the ones which are of practical interest.

It is shown that the algorithm is still valid if the transmitted chirp has a large time-bandwidth product BT.

3.5.1 Compensation algorithm for narrowband IF signals

Firstly, we attempt to carry over the derivation for temporally infinite chirps from Section 3.4 to a temporally *finite* one of the form

$$s_{TX}(t) = \text{rect}\left(\frac{t}{T}\right) \exp\left[j2\pi\left(f_c t + \frac{1}{2}\alpha t^2 + \epsilon(t)\right)\right], \tag{3.40}$$

where T is the sweep width, f_c the center frequency, α the sweep rate, and $\epsilon(t)$ is a phase error term in cycles (the phase error in radian is $2\pi\epsilon(t)$), The finite chirp (3.40) is thus the same as the infinite chirp (3.15) except for the pulse envelope $\text{rect}(t/T)$.

In analogy with Section 2.1.2, the received signal is simply delayed by the target transit time τ:

$$s_{RX}(t) = \text{rect}\left(\frac{t-\tau}{T}\right) \exp\left[j2\pi\left(f_c(t-\tau) + \frac{1}{2}\alpha(t-\tau)^2 + \epsilon(t-\tau)\right)\right]$$

(3.41)

Carrying over the steps in Section 2.1.3, the dechirped or intermediate frequency (IF) signal is now

$$\begin{aligned} s_{IF}(t) &= s_{TX}(t)s_{RX}^*(t) \\ &= r(t)\exp\left[j2\pi\left(f_c\tau + \alpha\tau t - \frac{1}{2}\alpha\tau^2 + \epsilon(t) - \epsilon(t-\tau)\right)\right], \end{aligned}$$

(3.42)

where $r(t)$ is the IF signal envelope given by (2.10).

We wish to apply the phase error compensation algorithm to the finite chirp. The first step, removal of the transmitted phase errors, can be applied just as in the temporally infinite case:

$$\begin{aligned} s_{IF2}(t) &= s_{IF}(t)s_\epsilon^*(t) \\ &= r(t)\exp\left[j2\pi\left(f_c\tau + \alpha\tau t - \frac{1}{2}\alpha\tau^2 - \epsilon(t-\tau)\right)\right]. \end{aligned}$$

(3.43)

Next, we apply the deskew filter to (3.43). Following the same steps as in the time-domain derivation (Section 3.4.4.2), we find

$$\begin{aligned} s_{IF3}(t) &= \exp[j2\pi(f_c\tau + \alpha\tau t)]\sqrt{j\alpha}\int_{-\infty}^{\infty} r(u)\exp[-j\pi\alpha(u-\tau-t)^2]\,s_\epsilon^*(u-\tau)du \\ &= \exp[j2\pi(f_c\tau + \alpha\tau t)]\sqrt{j\alpha}\int_{-\infty}^{\infty} r(v+\tau)\exp[-j\pi\alpha(t-v)^2]\,s_\epsilon^*(v)\,dv, \end{aligned}$$

(3.44)

the second line of which differs from (3.34) for the presence of a factor $r(v+\tau)$ in the convolution integral. As a result, the integral is not independent of τ as in the case of temporally infinite chirps.

We can still derive an approximate compensation algorithm, however, if we assume that the IF signal is narrowband as in Section 3.4.7. The integral in (3.44) can be seen to be the inverse Fresnel transform of the function $r(t+\tau)s_\epsilon^*(t)$:

$$\sqrt{j\alpha}\int_{-\infty}^{\infty} r(v+\tau)\exp[-j\pi\alpha(t-v)^2]\,s_\epsilon^*(v)\,dv = \{r(t+\tau)s_\epsilon^*(t)\} * q_{-\alpha}(t).$$

(3.45)

In Section 3.4.7, the its was shown that Fresnel transform of a function is approximately equal to the function itself if the function contains only low frequencies, such that its maximum frequency component is much less than $\sqrt{\alpha}$. It is easily seen that the same holds for the inverse Fresnel transform.

Let us consider the spectrum of the function $r(t+\tau)s_\epsilon^*(t)$. Since it is the convolution of the spectra of $r(t+\tau)$ and $s_\epsilon^*(t)$, its maximum frequency component will be the sum of the maximum frequency components of $r(t+\tau)$ and $s_\epsilon^*(t)$. Thus sum will be much less than $1/\sqrt{\alpha}$ if the respective maximum frequency components of $r(t+\tau)$ and $s_\epsilon^*(t)$ are individually much less than $1/\sqrt{\alpha}$.

Now, $r(t+\tau)$ is a rectangular analysis window of duration $T-\tau$, as illustrated in Figure 13(a). Its amplitude spectrum is a therefore a "sinc" function with peak-to-null distance $1/(T-\tau)$, as shown

in Figure 13(b). Since 90% of the energy of the "sinc" function is contained in the first lobe, we can say that the maximum frequency contained in the spectrum $R(f)$ of $r(t)$ is of the order of $1/(T - \tau) \approx 1/T$. (In practical applications, $\tau \ll T$). Therefore we obtain the requirement

$$\frac{1}{T} \ll \sqrt{\alpha} \tag{3.46}$$

or, rearranging and squaring both sides,

$$\alpha T^2 \gg 1. \tag{3.47}$$

The left hand side of (3.47) is simply equal to the time-bandwidth product BT of the temporally finite chirp. Hence, in addition to the requirement $f_{max} \ll \sqrt{\alpha}$ on the phase error function s_ϵ, we also have the requirement that the time-bandwidth product of the chirp must be large: $BT \gg 1$.
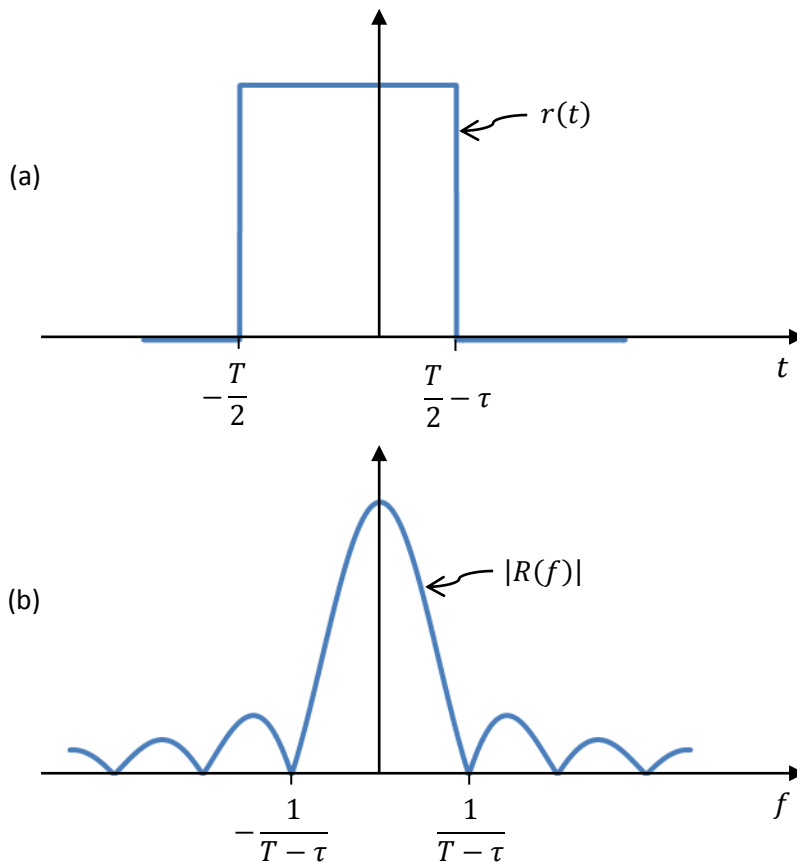
Figure 13 (a) Plot of the IF pulse envelope $r(t)$; (b) Plot of the amplitude spectrum $|R(f)|$ of $r(t)$. The maximum frequency component of $R(f)$ is seen to be of the order of $1/T$.

If the conditions (3.39) and (3.47) are fulfilled, then the stationary phase point of (3.44) is well approximated by $v \approx t$, so that, applying (3.7) to (3.44),

$$s_{IF3}(t) \approx r(t + \tau) \exp[j2\pi(f_c\tau + \alpha\tau t)] \, s_\epsilon^*(t). \tag{3.48}$$

In this narrowband approximation, the compensated signal is obtained by multiplying $s_{IF3}(t)$ by $s_\epsilon(t)$ to remove the residual phase errors:

$$s_{IF4}(t) = s_{IF3}(t)s_\epsilon(t)$$
$$\approx r(t+\tau)\exp[j2\pi(f_c\tau + \alpha\tau t)]. \tag{3.49}$$

In short, the approximate compensation method for narrowband IF signals described in Section 3.4.7 remains valid for finite chirps with large time-bandwidth products.

3.5.2   Application to sinusoidal phase errors

In the previous section, we essentially applied the stationary phase approximation to the deskew filtering convolution integral (3.45), and assumed that the stationary point was not affected by $r(t-\tau)s_\epsilon^*(t)$. However, if s_ϵ contains sufficiently high frequencies, the stationary point will change.

3.5.2.1   *Characterization of the phase error function*

To illustrate this effect, we assume the phase error $\epsilon(t)$ is sinusoidal, and has the form (cf. Section 2.2)

$$2\pi\epsilon(t) = A_{sl}\sin(2\pi f_{sl}t), \tag{3.50}$$

where A_{sl} is the phase error amplitude (in radian) and f_{sl} is the sidelobe ripple frequency. The corresponding error signal $s_\epsilon(t)$ is given by

$$s_\epsilon(t) \equiv \exp[j2\pi\epsilon(t)] = \exp[jA_{sl}\sin(2\pi f_{sl}t)]. \tag{3.51}$$

Since $s_\epsilon(t)$ is periodic with period $T_{sl} \equiv 1/f_{sl}$, it can be expressed as a Fourier series. It turns out that (Carson 1922)

$$s_\epsilon(t) = \sum_{n=-\infty}^{\infty} J_n(A_{sl})\exp(j2\pi n f_{sl}t), \tag{3.52}$$

where $J_n(\cdot)$ denotes the nth order Bessel function of the first kind, defined as

$$J_n(x) \equiv \frac{1}{2\pi}\int_{-\pi}^{\pi} e^{-j(nt-\sin t)}\,dt. \tag{3.53}$$

The first four Bessel functions are illustrated graphically in Figure 14.
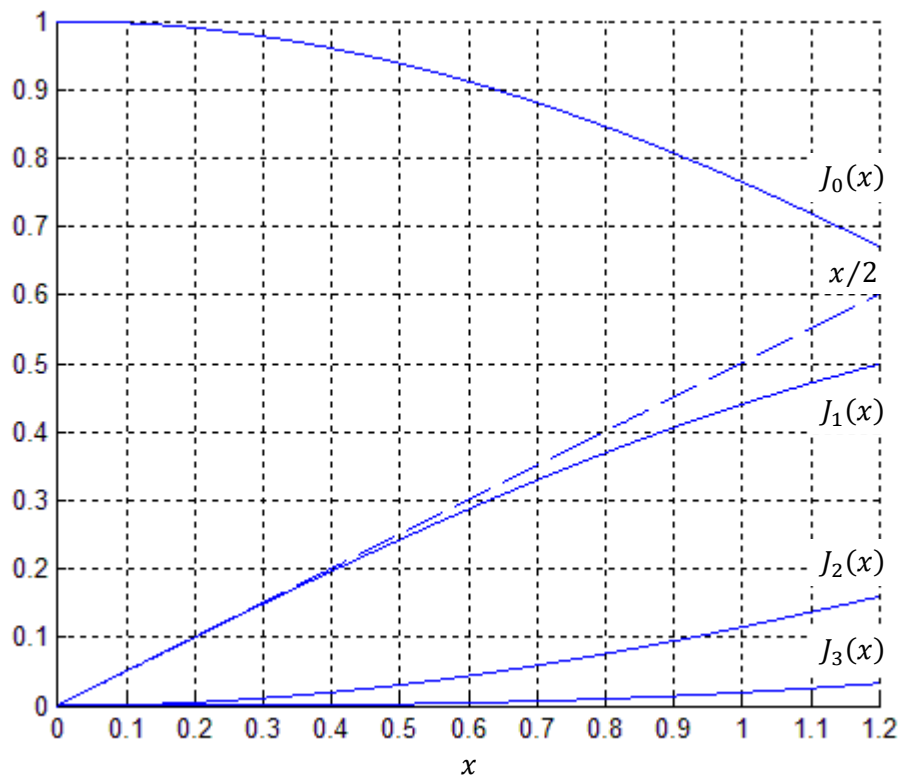
Figure 14 Bessel functions. (After (Klauder 1960)).

As seen from Figure 14, for A_{sl} small, we have the following approximations:

$$J_0(A_{sl}) \approx 1,$$ (3.54)(a)
$$J_1(A_{sl}) \approx A_{sl}/2,$$ (3.54)(b)
$$J_n(A_{sl}) \approx 0, \qquad n > 1.$$ (3.54)(c)

The approximations apply when (Klauder 1960)

$$A_{sl} < 0.4 \text{ radians}.$$ (3.55)

Further, using the identity

$$J_{-n}(x) = (-1)^n J_n(x),$$ (3.56)

we find that the error function $s_\epsilon(t)$ can be approximated by

$$s_\epsilon(t) \approx 1 + \frac{A_{sl}}{2}[\exp(j2\pi f_{sl}t) - \exp(-j2\pi f_{sl}t)].$$ (3.57)

(Note that, similarly to Section 2.2, (3.57) can also be obtained by expanding the exponential in (3.51) as a MacLaurin series, retaining only the first two terms, and using Euler's theorem to express the sine in terms of complex exponentials). In our subsequent calculations, we will assume a small-amplitude phase error (i.e., $A_{sl} \ll 1$) and invoke the approximation (3.57).

3.5.2.2   *Removal of the transmitted non-linearities*
In the first step of the phase error compensation method, the transmitted linearities $s_\epsilon(t)$ are removed:

$$s_{IF2}(t) = s_{IF}(t)s_\epsilon^*(t)$$
$$= r(t)s_{IF,lin}(t)s_\epsilon^*(t-\tau). \tag{3.58}$$

Inserting the small-angle approximation (3.57) into (3.58), we obtain

$$s_{IF2}(t) = r(t)e^{j2\pi\left(f_c\tau+\alpha\tau t-\frac{1}{2}\alpha\tau^2\right)}\left[1+\frac{A_{sl}}{2}\left(e^{-j2\pi f_{sl}(t-\tau)}-e^{j2\pi f_{sl}(t-\tau)}\right)\right]$$
$$\equiv s_{IF2,m}(t)+s_{IF2,l}(t)+s_{IF2,u}(t), \tag{3.59}$$

where $s_{IF2,m}$ is the 'main' signal at the desired beat frequency $\alpha\tau$:

$$s_{IF2,m}(t) = r(t)e^{j2\pi\left(f_c\tau+\alpha\tau t-\frac{1}{2}\alpha\tau^2\right)}, \tag{3.60}$$

$s_{IF2,l}$ is 'lower sidelobe' with amplitude $A_{sl}/2$ at frequency $\alpha\tau - f_{sl}$:

$$s_{IF2,l}(t) = \frac{A_{sl}}{2}r(t)e^{j2\pi\left((f_c+f_{sl})\tau+(\alpha\tau-f_{sl})t-\frac{1}{2}\alpha\tau^2\right)}, \tag{3.61}$$

and $s_{IF2,u}$ is an 'upper sidelobe' with amplitude $A_{sl}/2$ at frequency $\alpha\tau + f_{sl}$:

$$s_{IF2,u}(t) = -\frac{A_{sl}}{2}r(t)e^{j2\pi\left((f_c-f_{sl})\tau+(\alpha\tau+f_{sl})t-\frac{1}{2}\alpha\tau^2\right)}. \tag{3.62}$$

Thus, s_{IF2} is found to consist of a 'main' signal at the desired beat frequency $\alpha\tau$ with amplitude unity and two 'paired echoes' at $\alpha\tau \pm f_{sl}$ with amplitude $A_{sl}/2$.

Note that s_{IF2} has sidelobes with amplitudes $A_{sl}/2$, whereas the original IF signal s_{IF} has sidelobe levels $\beta/2$, where for long-wavelength phase errors ($\omega_{sl}\tau \ll 1$), $\beta = A_{sl}\omega_{sl}\tau$. Thus, for long-wavelength phase errors, the sidelobes in s_{IF2} are actually higher than those in s_{IF} by a factor $\omega_{sl}\tau$. (Of course, s_{IF2} is just an intermediate result; it is the sidelobe level in s_{IF4} that 'counts').

3.5.2.3 Deskew filtering
In the second step of the compensation algorithm, we pass s_{IF2} through a deskew filter to obtain a third beat signal, s_{IF3}:

$$s_{IF3}(t) = s_{IF2}(t) * q_{-\alpha}(t), \tag{3.63}$$

where (cf. (3.1))

$$q_{-\alpha}(t) = \sqrt{j\alpha}\exp(-j\pi\alpha t^2) \tag{3.64}$$

The output $s_{IF3}(t)$ consists of three terms, $s_{IF3,m}(t)$, $s_{IF3,l}(t)$, and $s_{IF3,u}(t)$ corresponding to the three terms $s_{IF2,m}(t)$, $s_{IF2,l}(t)$, and $s_{IF2,u}(t)$ of the input. We proceed to calculate these respective terms, invoking the stationary phase approximation.

The output corresponding to the 'main' IF signal is

$$s_{IF3,m}(t) = \sqrt{j\alpha}e^{j2\pi\left(f_c\tau-\frac{1}{2}\alpha\tau^2\right)}\int_{-\infty}^{\infty}r(t-t')e^{j2\pi\alpha\tau(t-t')}e^{-j\pi\alpha t'^2}dt'$$

$$= \sqrt{j\alpha}e^{j2\pi(f_c\tau+\alpha\tau t)}\int_{-\infty}^{\infty}r(t-t')e^{-j\pi\alpha(t'+\tau)^2}dt' \tag{3.65}$$

$$\approx r(t+\tau)e^{j2\pi(f_c\tau+\alpha\tau t)},$$

where the approximation in the last step,

$$\sqrt{j\alpha}e^{-j\pi\alpha t^2} \approx \delta(t), \tag{3.66}$$

is valid for chirps with large time-bandwidth product,

$$\alpha T^2 \gg 1, \tag{3.67}$$

and is justified by the same reasoning as in Section 3.5.1. (Note, however, that in this case we do not have the additional condition $f_{max} \ll \sqrt{\alpha}$, since there is no error function s_ϵ in the integrand of the second line of (3.65)). Thus, comparing (3.65) with (3.61), we see that the deskew filter shifts the envelope $r(t)$ of $s_{IF2}(t)$ backwards in time by τ seconds and imparts a phase shift of $\pi\alpha\tau^2$ radians to its carrier.

In a similar fashion, we obtain for the deskew-filtered lower sidelobe

$$s_{IF3,l}(t) = \frac{A_{sl}}{2}e^{j2\pi\left((f_c+f_{sl})\tau-\frac{1}{2}\alpha\tau^2\right)}\sqrt{j\alpha}\int_{-\infty}^{\infty}r(t-t')e^{j2\pi(\alpha\tau-f_{sl})(t-t')}e^{-j\pi\alpha t'^2}dt'$$

$$= \frac{A_{sl}}{2}e^{j2\pi(f_c\tau+(\alpha\tau-f_{sl})t)}\sqrt{j\alpha}\int_{-\infty}^{\infty}r(t-t')e^{-j\pi\alpha\left(t'^2+2\left(\tau-\frac{f_{sl}}{\alpha}\right)t'+\tau^2-2\frac{f_{sl}}{\alpha}\tau\right)}dt' ;$$

'Completing the square' in the complex exponential in the integrand, we find

$$s_{IF3,l}(t) = \frac{A_{sl}}{2}e^{j2\pi\left(f_c\tau+(\alpha\tau-f_{sl})t+\frac{1}{2}\frac{f_{sl}^2}{\alpha}\right)}\sqrt{j\alpha}\int_{-\infty}^{\infty}r(t-t')e^{-j\pi\alpha\left(t'+\tau-\frac{f_{sl}}{\alpha}\right)^2}dt'. \tag{3.68}$$

Applying the stationary phase approximation to (3.68)

$$s_{IF3,l}(t) \approx \frac{A_{sl}}{2}r\left(t+\tau-\frac{f_{sl}}{\alpha}\right)e^{j2\pi\left(f_c\tau+(\alpha\tau-f_{sl})t+\frac{1}{2}\frac{f_{sl}^2}{\alpha}\right)}. \tag{3.69}$$

Thus, comparing (3.69) with (3.61), we see that the deskew filter shifts envelope $r(t)$ of the lower sidelobe of $s_{IF2,l}(t)$ backwards in time by $\tau - f_{sl}/\alpha$ seconds (f_{sl}/α seconds less than the 'main' signal) and acquires a phase shift of $\pi(\alpha\tau - f_{sl})^2/\alpha$ radians to its carrier.

In an analogous fashion, we find for the upper sidelobe

$$s_{IF3,u}(t) \approx -\frac{A_{sl}}{2}r\left(t+\tau+\frac{f_{sl}}{\alpha}\right)e^{j2\pi\left(f_c\tau+(\alpha\tau+f_{sl})t+\frac{1}{2}\frac{f_{sl}^2}{\alpha}\right)}. \tag{3.70}$$

Thus, comparing (3.70) with (3.62), we see that the deskew filter shifts envelope $r(t)$ of the lower sidelobe of $s_{IF2,l}(t)$ backwards in time by $\tau + f_{sl}/\alpha$ seconds (f_{sl}/α seconds more than the 'main' signal) and acquires a phase shift of $\pi(\alpha\tau + f_{sl})^2/\alpha$ radians to its carrier.

Finally, adding the contributions (3.65), (3.69), and (3.70), we find

Finally, adding the contributions (3.65), (3.69), and (3.70), we find

$$
\begin{aligned}
s_{IF3}(t) &= s_{IF3,m}(t) + s_{IF3,l}(t) + s_{IF3,u}(t) \\
&= r(t+\tau)e^{j2\pi(f_c\tau+\alpha\tau t)} + \frac{A_{sl}}{2}r\left(t+\tau-\frac{f_{sl}}{\alpha}\right)e^{j2\pi\left(f_c\tau+(\alpha\tau-f_{sl})t+\frac{1}{2}\frac{f_{sl}^2}{\alpha}\right)} \\
&\quad - \frac{A_{sl}}{2}r\left(t+\tau+\frac{f_{sl}}{\alpha}\right)e^{j2\pi\left(f_c\tau+(\alpha\tau+f_{sl})t+\frac{1}{2}\frac{f_{sl}^2}{\alpha}\right)}.
\end{aligned}
\tag{3.71}
$$

Thus, the deskew-filtered signal $s_{IF3}(t)$ comprises three terms, each offset slightly in both frequency an time.

It is interesting to reflect on how the terms in (3.71) an be derived in a simpler fashion. Recall that the transfer function of the deskew filter is given by

$$
Q_{-\alpha}(f) = \exp\left(j\frac{\pi}{\alpha}f^2\right) \equiv \exp[j\Phi_{-\alpha}(f)].
\tag{3.72}
$$

The envelopes, $r(t)$, of $s_{IF2,m}(t)$, $s_{IF2,l}(t)$, and $s_{IF2,u}(t)$ are delayed by the filter group delay,

$$
t_{g,-\alpha} = -\frac{1}{2\pi}\frac{d\Phi_{-\alpha}}{df} = -\frac{f}{\alpha},
\tag{3.73}
$$

evaluated at their respective frequencies $\alpha\tau$, $\alpha\tau - f_{sl}$, and $\alpha\tau + f_{sl}$. As for the complex exponential phase factors of $s_{IF2,m}(t)$, $s_{IF2,l}(t)$, and $s_{IF2,u}(t)$, these are multiplied by the deskew filter frequency response $Q_{-\alpha}(f)$ evaluated at these frequencies.

3.5.2.4 Restriction to an interval not affected by the finite nature of the chirp

On the interval $[-T/2+f_{sl}/\alpha, T/2-\tau-f_{sl}/\alpha]$, the envelopes of the three terms in (3.71) are all equal to unity, and we have

$$
\begin{aligned}
s_{IF3}(t) &= e^{j2\pi(f_c\tau+\alpha\tau t)}\left[1 + \frac{A_{sl}}{2}e^{j\pi\frac{f_{sl}^2}{\alpha}}\left(e^{-j2\pi f_{sl}t} - e^{j2\pi f_{sl}t}\right)\right] \\
&= e^{j2\pi(f_c\tau+\alpha\tau t)}\left[1 - jA_{sl}e^{j\pi\frac{f_{sl}^2}{\alpha}}\sin(2\pi f_{sl}t)\right], \qquad -\frac{T}{2}+\frac{f_{sl}}{\alpha} < t < \frac{T}{2}-\tau-\frac{f_{sl}}{\alpha}.
\end{aligned}
\tag{3.74}
$$

Thus on this limited interval the signal is (to within the stationary phase approximation) the same as if the chirp were temporally infinite.

3.5.2.5 Removal of the residual phase errors

In order to perform the next step of the phase error compensation algorithm, we compute

$$
s_{\epsilon,\alpha}(t) = s_\epsilon(t) * q_\alpha(t),
\tag{3.75}
$$

where $h_\alpha(t)$ is the 'skew' filter with transfer function and frequency response

$$
q_\alpha(t) = \sqrt{-j\alpha}\exp(j\pi\alpha t^2) \leftrightarrow \exp\left(-j\frac{\pi}{\alpha}f^2\right) = Q_\alpha(f).
\tag{3.76}
$$

Note that in the sign of α is reversed with respect to the transfer function $q_{-\alpha}(t)$ of the 'deskew' filter.

With the error function given by (3.57), it can be shown that

$$s_{\epsilon,\alpha}(t) = 1 + \frac{A_{sl}}{2} e^{-j\pi\frac{f_{sl}^2}{\alpha}} \left(e^{j2\pi f_{sl}t} - e^{-j2\pi f_{sl}t}\right)$$
$$= 1 + jA_{sl}e^{-j\pi\frac{f_{sl}^2}{\alpha}} \sin(2\pi f_{sl}t). \tag{3.77}$$

Multiplying (3.74) and (3.77) and neglecting terms in A_{sl}^2, we find

$$s_{IF4}(t) = e^{j2\pi(f_c\tau+\alpha\tau t)} \left[1 + jA_{sl}e^{-j\pi\frac{f_{sl}^2}{\alpha}} \sin(2\pi f_{sl}t) - jA_{sl}e^{j\pi\frac{f_{sl}^2}{\alpha}} \sin(2\pi f_{sl}t)\right],$$
$$-\frac{T}{2} + \frac{f_{sl}}{\alpha} < t < \frac{T}{2} - \tau - \frac{f_{sl}}{\alpha}. \tag{3.78}$$

Now, provided that

$$f_{sl} \ll \sqrt{\alpha} \tag{3.79}$$

the exponential terms in the square brackets in (3.78) will be close to unity, whence the second and third terms in square brackets in (3.78) and we obtain

$$s_{IF4}(t) \approx e^{j2\pi(f_c\tau+\alpha\tau t)}, \qquad -\frac{T}{2} + \frac{f_{sl}}{\alpha} < t < \frac{T}{2} - \tau - \frac{f_{sl}}{\alpha}. \tag{3.80}$$

It is important to note that the interval in (3.80) on which the compensated output is obtained is *shorter*, by $2f_{sl}/\alpha$, than the interval on which it would be observed if there were no sinusoidal phase error. Physically, this is because deskew filter applies different group delays to each original 'paired echo', so that the 'paired echoes' at the output of the filter have less temporal overlap. This effect could be of importance in our simulations, as we discuss in Section 4.5.

4 Simulation

In this chapter, we simulate a signal processor implementing the phase error compensation algorithm in order to verify the results derived in Chapter 3. The key part of the algorithm is the deskew filter. Following Eichel et al. (Eichel 2005), we implement the filter in the frequency domain using the *frequency sampling method*.

This chapter is organized as follows. In Section 4.1, we give an overview of the digital implementation of the phase error compensation algorithm. In Section 4.2, we describe the implementation of the digital deskew filter, and test it against a known exact solution. Finally, in Section .., we present the full algorithm.

4.1 Digital implementation of the phase error compensation method

The digital implementation of the phase error is illustrated in Figure 15. The input to the algorithm is are samples of the coherently detected intermediate frequency (IF) signal, which appears as a finite array of complex numbers, $s_{IF}[n]$. This array is multiplied, element-by-element, with the sampled values of the complex conjugate of the error function, $s_\epsilon^*[n]$, to remove phase errors emanating from the transmitted signal. The thus obtained array $s_{IF2}[n]$ is passed through a digital deskew filter, described in Section 4.2, to obtain an output array $s_{IF3}[n]$ in which the residual phase errors from the received signal are time-aligned. Finally, $s_{IF3}[n]$ is multiplied element-by-element with the residual phase error function $s_{\epsilon,\alpha}[n]$ to remove the residual phase errors.
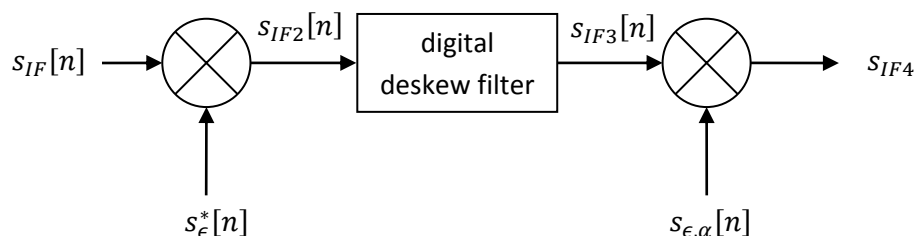
Figure 15 Digital implementation of the phase error compensation method.

The crucial part in the algorithm is the digital deskew filter to time align the phase errors in the received echoes. Because it is a dispersive filter, the output is translated and 'spread' in time. This calls for a different approach to the digital filter design than that used for frequency-selective finite impulse response (FIR) filters commonly discussed in the literature (Oppenheim, Schafer et al. 1999), which can be made to have linear phase.

4.2 Implementation of the deskew filter by the frequency sampling method

We implement the digital deskew filter using the frequency sampling method. This includes the steps of performing the FFT on the deramped data, multiplying the result of the FFT on a sample-by-sample basis with a pre-computed and pre-stored deskew vector, and performing the inverse FFT.

An artifact that commonly occurs in frequency sampling is *time-domain aliasing*, which is analogous to the frequency-domain aliasing phenomenon in spectral estimation. In order to prevent time-

domain aliasing from corrupting the filter output, the frequency sample spacing must be chosen sufficiently small. This, in turn, requires that the FFT on the deramped data be performed after padding it with a sufficient number of zeroes.

The organization of this section is as follows. In Subsection 4.2.1, we discuss the phenomenon of time-domain aliasing in a general setting. In Subsection 4.2.2, we quantify the number of FFT points required to prevent time-domain aliasing in a digital deskew filter implementation. Subsequently, we describe the FFT implementation of the steps described in Section 4.1: approximation of the spectrum of the input signal (Subsection 4.2.3), multiplication of the thus obtained approximation by the exact deskew filter frequency response (Subsection 4.2.4), and using the thus obtained frequency samples to approximate the filter output on a desired interval (Subsection 4.2.5). Finally, in Subsection , we put the results of Subsections 4.2.3-4.2.5 together to

4.2.1　The frequency sampling method and time-domain aliasing

Consider the ideal case that a continuous-time input[16] $x(t)$ is passed through a deskew filter with frequency response $Q_{-\alpha}(f)$. The continuous-time output $y(t)$ in this case is given by the inverse Fourier transform of $X(f)Q_{-\alpha}(f)$, i.e.,

$$y(t) = \int_{-\infty}^{\infty} X(f)Q_{-\alpha}(f)e^{j2\pi ft}df. \tag{4.1}$$

Now suppose we approximate this integral by a Riemann sum to obtain an approximate output $\bar{y}(t)$:

$$\bar{y}(t) \equiv \Delta f \sum_{k=-\infty}^{\infty} X(k\Delta f)Q_{-\alpha}(k\Delta f)\exp(j2\pi k\Delta ft), \tag{4.2}$$

where Δf is the frequency sample spacing. For Δf sufficiently small, we would expect $y(t) \approx \bar{y}(t)$; we derive the form of the error presently.

The Riemann sum (4.2) can be expressed in the form of an inverse Fourier transform as follows:

$$\bar{y}(t) = \int_{-\infty}^{\infty} \left[\Delta f \sum_{k=-\infty}^{\infty} \delta(f - k\Delta f) \right] X(f)Q_{-\alpha}(f)e^{j2\pi ft}df. \tag{4.3}$$

The expression between square brackets in (4.3) represents a train of Dirac delta functions in the frequency domain spaced Δf Hertz apart, each with a gain of Δf Hertz. The multiplication of the convolution kernel $X(f)Q_{-\alpha}(f)$ by this impulse train effects the conversion of the inverse Fourier integral (4.1) into the Reimann sum (4.2).

It can be shown (Bracewell 1986) that the inverse Fourier transform of the expression in square brackets in (4.3) is a train of Dirac delta functions in the time domain with spacing $1/\Delta f$ seconds and a gain of unity:

---

[16] For the sake of generality and brevity, we use x and y here to denote the deskew filter input and output, respectively. (In the implementation of the phase error compensation algorithm, the deskew filter is actually used twice: once per sweep ('on-line') to compute s_{IF3} from s_{IF2}, and once beforehand ('off-line') to compute $s_{\epsilon,-\alpha}$ from s_{ϵ}. The general output y and input x thus represents either one of these pair of signals).

$$\Delta f \sum_{k=-\infty}^{\infty} \delta(f - k\Delta f) \leftrightarrow \sum_{n=-\infty}^{\infty} \delta\left(t - \frac{n}{\Delta f}\right). \tag{4.4}$$

Thus, applying the convolution theorem to (4.3) and substituting (4.1) and (4.4), the Riemann sum $\bar{y}(t)$ can be expressed as

$$\bar{y}(t) = y(t) * \sum_{n=-\infty}^{\infty} \delta\left(t - \frac{n}{\Delta f}\right) = \sum_{n=-\infty}^{\infty} y\left(t - \frac{n}{\Delta f}\right), \tag{4.5}$$

where we have used the "sifting property" of the Dirac delta function in the second step (Bracewell 1986). Hence, the output will consist of a periodic repetition of the desired output $y(t)$ with period $1/\Delta f$. It follows that in order to prevent the aliases from overlapping each other, the duration of $y(t)$ must be smaller than $1/\Delta f$.

4.2.2 Number of FFT points required to prevent time-domain aliasing

Now suppose that the input $x(t)$ is sampled at a rate f_s, and N complex samples are collected over a period $T_x = N/f_s$. Suppose that these samples are used to approximate the spectrum $X(f)$ of $x(t)$ on the Nyquist interval $(-f_s/2, f_s/2)$.

Consider the effect of applying the deskew filter with frequency response $Q_{-\alpha}(f)$ to the input $x(t)$. As mentioned earlier, the filter has a group delay of $t_{g,\alpha}(f) = -f/\alpha$. Therefore, the frequency component at $f_s/2$ will experience a delay of $-f_s/2\alpha$, whereas the one at $-f_s/2$ will experience one of $f_s/2\alpha$. This difference will cause the input pulse to widen by the amount f_s/α. So the width of the output will be

$$T_y = T_x + \frac{f_s}{\alpha}. \tag{4.6}$$

Now, if we extend the FFT operation from N to N_{FFT} points, then the frequency spacing Δf will be

$$\Delta f = \frac{N}{N_{FFT} T_x}. \tag{4.7}$$

In order to prevent the time-domain aliases from overlapping each other, we must have

$$T_y < \frac{1}{\Delta f}$$

or, inserting (4.6) and (4.7) and rearranging,

$$N_{FFT} > N\left(1 + \frac{f_s}{\alpha T_x}\right). \tag{4.8}$$

Using the fact that $T_x = N/f_s$, (4.8) can alternatively be expressed as

$$N_{FFT} > N + \frac{f_s^2}{\alpha}. \tag{4.9}$$

Therefore, in order to prevent time-domain aliasing, the number of FFT points N_{FFT} must be chosen larger than the sum of the number of samples N and the quantity f_s^2/α, where f_s is the sampling frequency and α the chirp rate of the quadratic phase filter. (This criterion can be relaxed somewhat

if the input signal is oversampled, i.e., does not contain frequency components all the way up to its Nyquist frequency).

4.2.3   Approximating the input signal spectrum

As indicated in Section 4.1, the first step in the frequency sampling implementation of the deskew filter is to approximate the spectrum $X(f)$ of the input signal $x(t)$.

Regarding the input as time-limited to the sweep interval $[-T/2, T/2]$, we want to find the spectrum of a time-limited function $x(t)$:

$$X(f) = \int_{-T/2}^{T/2} x(t)e^{-j2\pi ft} dt. \tag{4.10}$$

Defining the grid points

$$t_n = -\frac{T}{2} + nT_s, \qquad n = 0,1,\dots,N-1 \tag{4.11}$$

where

$$T_s \equiv \frac{T}{N} \tag{4.12}$$

is the sampling period, we approximate the integral in (4.10) as a left-hand Riemann sum[17], to obtain an approximation $\bar{X}(f)$ of the exact spectrum $X(f)$:

$$\begin{aligned}
\bar{X}(f) &\equiv T_s \sum_{n=0}^{N-1} x(t_n)e^{-j2\pi ft_n} \\
&= T_s(-1)^{fT} \sum_{n=0}^{N-1} x(t_n)e^{-j2\pi fn\frac{T}{N}},
\end{aligned} \tag{4.13}$$

where we have substituted (4.11) to obtain the second line.

The function $\bar{X}(f)$ given by (4.13) is at this point still a continuous function of frequency, f. A digital signal processor, however, can only output an array of sampled values of this function, due to its discrete nature. We choose to evaluate $\bar{X}(f)$ on the following array of points:

$$f_k = f_s\left(-\frac{1}{2} + \frac{k}{N_{FFT}}\right), \qquad k = 0,1,\dots,N_{FFT}-1, \tag{4.14}$$

where

---

[17] The Riemann sum $\bar{X}(f)$ given by (4.13) is only a first-order accurate approximation of the exact signal spectrum $X(f)$. Several methods for obtaining higher-order accuracy have been proposed in the literature (see, for example, (Press, Teukolsky et al. 2007)). Although higher-order accuracy would be desirable in a real-time implementation of the PEC algorithm, in this thesis we are interested in providing a "proof of principle", and therefore we have chosen to use the simpler, first-order accurate formula (4.13).

$$f_s \equiv \frac{N}{T} = \frac{1}{T_s} \qquad (4.15)$$

is the sampling frequency. The array (4.14) thus represents a partition of the *Nyquist interval* $(-f_s/2, f_s/2)$ into N_{FFT} sub-intervals, so that the frequency sample spacing is f_s/N_{FFT} as required.

Evaluating the approximation $\bar{X}(f)$ given by (4.13) on the grid points f_k given by (4.14), we find

$$\bar{X}(f_k) = \frac{T}{N}(-1)^{f_k T} \sum_{n=0}^{N-1} (-1)^n x(t_n) \exp\left(-\frac{j2\pi kn}{N_{FFT}}\right). \qquad (4.16)$$

For $k = 0, 1, \ldots, N_{FFT} - 1$, the sum in (4.16) this has the standard form of an N_{FFT}-point FFT as implemented by MATLAB®, for example.

Mathematical symbol	MATLAB symbol
$\bar{X}(f_k), \ k = 0, 1, \ldots, N_{FFT} - 1$	X
$x(t_n), \ n = 0, 1, \ldots, N - 1$	x
$f_k, \ k = 0, 1, \ldots, N_{FFT} - 1$	f
$[0, 1, \ldots, N - 1]$	n
$[0, 1, \ldots, N_{FFT} - 1]$	k
N, N_{FFT}	N, NFFT

Table 3 Mathematical expressions and their corresponding MATLAB symbols.

Identifying the mathematical expressions in (4.16) with MATLAB symbols as in Table 3, the spectrum $X(f)$ can be approximated at the points f_k given by (4.14) by the following line of MATLAB code:

```
X=T/N*(-1).^(f*T).*fft(x.*(-1).^n,NFFT);                          (4.17)
```

A short explanation of the code is as follows. In MATLAB, the symbols ".*" and ".^" denote the array (i.e., element-by-element) multiplication and array power operations, respectively. Further, the operation `fft(s,NFFT)` on an array `s` produces the `NFFT`-point discrete Fourier transform (DFT) of that array. In our case in which the FFT length is larger than the array length (`NFFT>N`), this means that the so the input array `s` is padded with `NFFT−N` trailing zeroes prior to performing the DFT.

4.2.4 Multiplication by the exact deskew filter frequency response

Thus, the digital spectrum $\bar{X}(f)$ of the input signal is approximated at discrete points f_k on the Nyquist interval $(-f_s/2, f_s/2)$. This is multiplied by the deskew filter transfer function evaluated at these points to obtain the output $\bar{Y}(f_k)$:

$$\begin{aligned} \bar{Y}(f_k) &= \bar{X}(f_k) Q_{-\alpha}(f_k) \\ &= \bar{X}_k \exp\left(j\frac{\pi}{\alpha} f_k^2\right). \end{aligned} \qquad (4.18)$$

This gives an approximation of the output on the Nyquist interval $(-f_s/2, f_s/2)$.

In MATLAB code, this is implemented as follows:

```
Y=X.*exp(1j*pi*f.^2/alpha);                                       (4.19)
```

Here `fs = N/T` is the sampling rate, and `alpha` ('mathematical' symbol: α) is the chirp rate of the deskew filter.

4.2.5 Inverse Fourier transform of the spectrum of the output

Next, we wish to take the inverse Fourier transform of $\bar{Y}(f)$ to obtain an approximate output $\bar{y}(t)$:

$$\bar{y}(t) = \int_{-f_s/2}^{f_s/2} \bar{Y}(f) \exp(j2\pi ft)\, df. \tag{4.20}$$

Approximating this integral by a Riemann sum, we obtain an approximation $\hat{y}(t)$ of $\bar{y}(t)$:

$$\hat{y}(t) = \frac{f_s}{N_{FFT}} \sum_{k=0}^{N_{FFT}-1} Y(f_k) \exp(j2\pi f_k t). \tag{4.21}$$

Inserting the expression for the f_k, equation (4.14), into (4.21) yields

$$\hat{y}(t) = \frac{f_s(-1)^{f_s t}}{N_{FFT}} \sum_{k=0}^{N_{FFT}-1} Y(f_k) \exp\left(\frac{j2\pi k f_s t}{N_{FFT}}\right) \tag{4.22}$$

Evaluating $\hat{y}(t)$ at the time points t_n given by (4.11), and again assuming that N contains more than one prime factor of 2, we find

$$\hat{y}(t_n) = f_s(-1)^{-f_s t_n} \left[\frac{1}{N_{FFT}} \sum_{k=0}^{N_{FFT}-1} (-1)^{\frac{kN}{N_{FFT}}} Y(f_k) \exp\left(j2\pi \frac{kn}{N_{FFT}}\right) \right]. \tag{4.23}$$

The term between square brackets has the MATLAB form of a N_{FFT}-point *inverse* DFT. Thus, the filter output for $n = 0, \dots, N-1$ is obtained by the following MATLAB code:

```
y=fs*(-1).^(fs*t).*ifft((-1).^(k*N/NFFT).*Y,NFFT);

y=y(1:N);
```
(4.24)

The first line in (4.24) computes an N_{FFT}-point inverse DFT. The first N points of this represent the desired output.

4.2.6 Implementation of the deskew filter as a MATLAB function

The results of the previous subsections can be combined to a concise MATLAB code. After combining the steps described above, the output of the digital deskew filter with chirp rate α on input sampled at a rate f_s is found to depend on the dimensionless parameter

$$A = \frac{\alpha}{f_s^2}. \tag{4.25}$$

A listing of our MATLAB function, deskew, is given below in nine lines of code.

```
1  function y=deskew(x,A)
2  N=length(x);
3  NFFT=2^nextpow2(N+1/abs(A));
4  n=0:N-1;
5  k=0:NFFT-1;
6  X=exp(1j*pi*N*(-1/2+k/NFFT)).*fft(x.*(-1).^n,NFFT);
7  Y=X.*exp(1j*pi*(-1/2+k/NFFT).^2/A);
8  y=exp(1j*pi*(N/2-k)).*ifft(Y.*exp(-1j*pi*k*N/NFFT),NFFT);
9  y=y(1:N);
```

A short explanation of the code is as follows. In line 3, we choose the number of FFT points as the next power of 2 larger than $N + f_s^2/\alpha = N + 1/A$, as specified in Subsection 4.2.2. Lines 4 and 5 define the discrete-time indices n and k corresponding to the time samples t_n and frequency samples f_k, respectively. Line 6 is an implementation of (4.16) in which a factor T_s has been omitted, since this factor later cancels against a factor f_s which would be required in line 8. Line 7 is an implementation of (4.19), in which the factor f_s in the definition of the f_k is combined with the factor $1/\alpha$ to 1/A. Lines 8 and 9 are an implementation of (4.24), where a pre-factor f_s has been omitted as explained earlier.

4.2.7 Test of the deskew filter for a known, exact output

We have tested the deskew filter for the case in which the IF signal is the linear IF signal, not perturbed by phase errors:

$$s_{IF}(t) = r(t) \exp\left(j2\pi \left(f_c\tau - \frac{1}{2}\alpha\tau^2 + \alpha\tau t \right) \right) \tag{4.26}$$

The deskew filter output in this case is

$$s_{IF}(t) = \exp[j2\pi(f_c\tau + \alpha\tau t)] \sqrt{\frac{j}{2}} \left[Z^*\left(\sqrt{2\alpha}\left(t + \frac{T}{2} \right) \right) - Z^*\left(\sqrt{2\alpha}\left(t - \frac{T}{2} + \tau \right) \right) \right]. \tag{4.27}$$

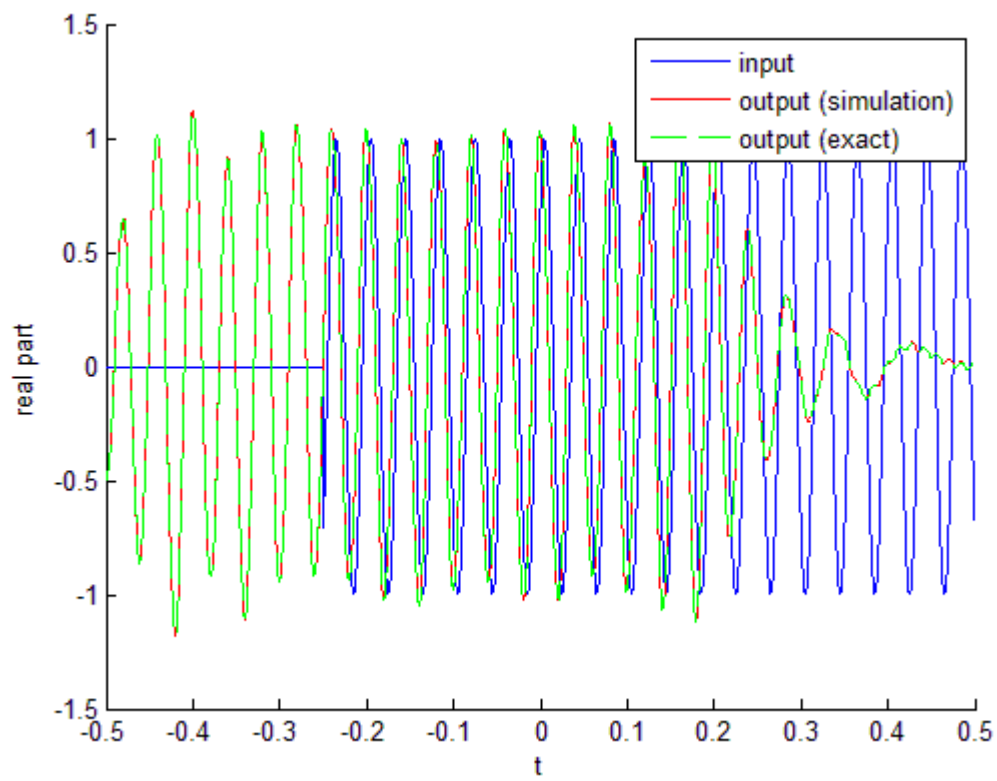A comparison of these two functions is shown below.

Figure 16 Real part of the input (blue line) and deskew filter output (red, green lines) for a time-bandwidth product of 100.
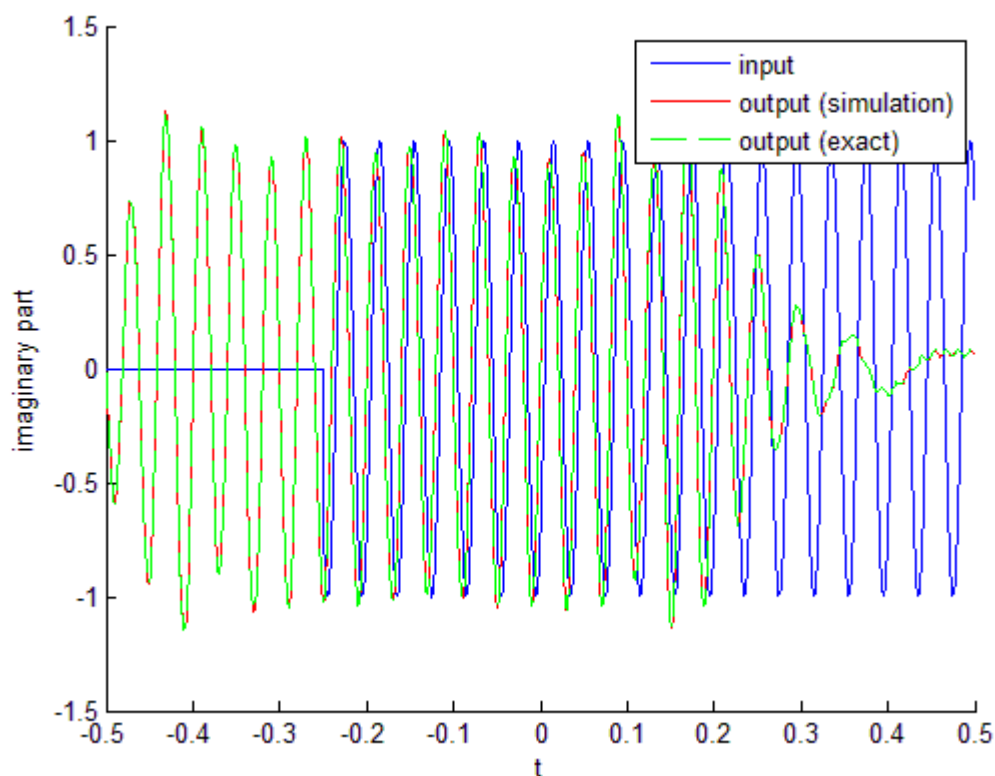
Figure 17 Imaginary part of the input (blue line) and deskew filter output (red, green lines) for a time-bandwidth product of 100.

Thus, we have designed and validated the digital deskew filter. We proceed to apply it in a full simulation of the phase error compensation algorithm.

4.3   Simulation of the phase error compensation algorithm

We have applied the ideas outlined above in a full MATLAB simulation of the phase error compensation algorithm. The MATLAB code for the simulation is given and explained in the Appendix. In this section, we enumerate the parameters used the simulation and present a flow diagram of the calculations.

The parameters used for the simulation are tabulated in Table 4[18]. In our application, N = 12,500 samples are collected at a rate of f_s = 25 MHz during each sweep repetition interval T = 500 μs. This sample rate f_s is more than twice the maximum beat frequency, $f_{b,max}$ = 10 MHz, as required by the Nyquist sampling criterion (see Section 2.1.4). The first 2,500 samples, which correspond to the initial τ_{max} of each sweep period and are affected by 'fly-backs' from the previous sweep, are set to

---

[18] We have chosen parameters similar to those of the first commercial FMCW radar, the PILOT (**P**hilips **I**ndetectable **L**ow **O**utput **T**ransceiver), which was first marketed in 1988 by the then Philips' subsidiaries Signaal in the Netherlands and Bofors in Sweden {Pace, 2009 #344}. Our FFT size, however, is much larger than in the original PILOT radar, where a 1,024-point FFT was used.

zero, so that the number of *processed* samples is N_p = 10,000. The processed samples are padded with zeroes up to a FFT length of 2^{15} = 32,768 to obtain fine frequency resolution[19].

Parameter	Symbol / Formula	Value	Unit
RF center frequency	f_c	10	GHz
RF wavelength	λ_c	30	mm
Frequency excursion, peak-to-peak	B	50	MHz
Ideal time resolution	$1/B$	20	ns
Ideal range resolution	$c/2B$	3	m
Sweep repetition interval (SRI)	T	500	µs
Sweep repetition frequency (SRF)	$1/T$	2	kHz
Sweep rate	α	100	GHz/s
Beat frequency / range ratio	$2B/cT$	6.67	kHz/m
Range / beat frequency ratio	$cT/2B$	0.15	m/kHz
Maximum ('instrumented') range	R_{max}	15	km
Maximum transit time	τ_{max}	100	µs
Maximum beat frequency	$f_{b,max}$	10	MHz
Minimum beat frequency interval	$T - \tau_{max}$	400	µs
Minimum beat frequency spectral width	$1/(T - \tau_{max})$	2.5	kHz
Minimum range resolution	$cT/[2B(T - \tau_{max})]$	3.75	m
ADC sample rate	f_s	25	MHz
ADC sampling period	T_s	40	ns
ADC sampling interval	T_{AD}	400	µs
Number of samples collected per sweep	N	12,500	samples
Number of processed samples per sweep	N_p	10,000	samples
FFT length	N_{FFT}	32,768	samples
FFT frequency sample spacing	f_s/N_{FFT}	0.763	kHz
FFT range sample spacing	$(cT/2B)(f_s/N_{FFT})$	1.14	m
Window	Hamming		
Window frequency resolution (6 dB)		1.81	sample
Window frequency resolution (6 dB)		4.53	kHz
Window range resolution (6 dB)		6.79	m

Table 4 FMCW radar parameters. (After {Piper, 1993 #4}).

In Figure 18, we show a flow diagram of the calculations performed in the simulation. The input to the simulation is the "uncompensated" beat signal $s_{IF}(t)$ as given by equation (3.42), which is affected by specified phase errors $\epsilon(t)$. The simulation calculates four output spectra; from left to right at the bottom of Figure 18, these are:

1) A "wideband" compensated beat signal spectrum $S_{IF4,w}$, which follows the algorithm by Meta et al. {Meta, 2007 #46} described in Sections 3.4.3-3.4.5;
2) A "narrowband" compensated beat signal spectrum $S_{IF4,w}$ which follows the algorithm of Burgos-Garcia et al. {Burgos-Garcia, 2003 #341} described in Section 3.4.7;
3) An "uncompensated" beat signal spectrum S_{IF} calculated by the observed beat signal s_{IF} which is affected by phase errors; and

---

[19] We have chosen to evaluate the final range FFT using the same number of points as required for the deskew filtering by equation (4.9).

4) An "ideal" beat signal spectrum $S_{IF,lin}$ calculated from the ideal beat signal $s_{IF,lin}$ given by (3.13).

The beat signals are windowed prior to performing the range FFT. Since the deskew filter effectively translates the beat signal in time, different window functions are used for the compensated signals ($s_{IF4,w}$ and $s_{IF4,n}$) and the uncompensated signals (s_{IF} and $s_{IF,d}$). The uncompensated signals use a Hamming window w_{IF} with support on the interval $[-T/2+\tau, T/2)$. The compensated signals, however, use a Hamming window w_{IF4} shifted τ seconds to the left, which thus has support on the interval $[-T/2, T/2-\tau)$.

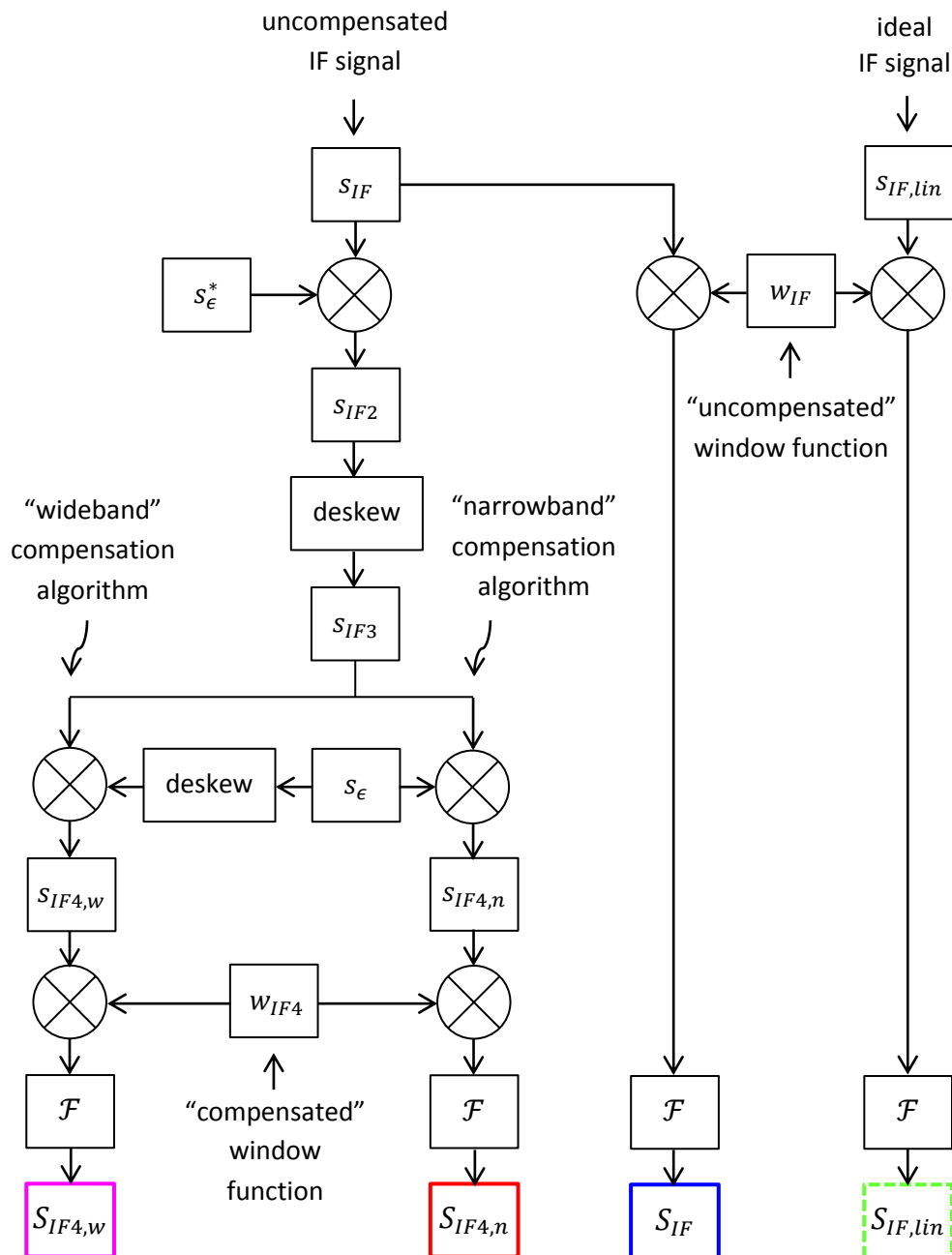**Figure 18 Flow diagram of the simulation. The crossed circles represent multiplications, the "deskew" blocks represent deskew filtering, and the "$\mathcal{F}$" blocks represent (approximate) Fourier transformation. The remaining blocks represent**

An important aspect of the flow diagram shown above is that we have applied the *deskew* (not skew) filter to the function s_ϵ in order to obtain remove the residual phase errors in the last step of the "wideband" compensation algorithm. This corresponds to the algorithm as originally formulated by Meta {Meta, 2007 #46}, and was found to give better results in our simulations for sinusoidal phase errors in Section 4.4.1. However, it is at odds with our analytical derivations in Chapter 3. We return to this point in Section 4.5. (Note that if the phase error function contains only low frequencies such that (3.39) is satisfied, then either variety of the algorithm will work, since in this case $s_{\epsilon,\alpha} \approx s_{\epsilon,-\alpha} \approx s_\epsilon$ by virtue of (3.8)).

In the MATLAB code implementing the simulation, the phase error $\epsilon(t)$ is specified on a separate line as an in-line function. By changing this in-line function, we can apply the phase error compensation algorithms to any phase error we like. The results for a number of phase errors are described presently.

4.4   Results for cases of interest

The MATLAB code described in Section 4.3 was used to simulate the performance of both the "wideband" and the "narrowband" compensation algorithm for a number of cases of interest.

4.4.1   Sinusoidal phase errors

We have performed simulations using a sinusoidal phase error of the form (cf. (2.18))

$$2\pi\epsilon(t) = A_{sl}\sin(2\pi f_{sl}t), \qquad (4.28)$$

where A_{sl} represents the peak phase error (in radian), and f_{sl} the sidelobe ripple frequency. The performance of the compensation algorithms depends on these parameters, as we show presently.

4.4.1.1   *Low-frequency phase error ($f_{sl} \ll \sqrt{\alpha}$)*

First, we investigate the case in which the $A_{sl} \ll 1$ and $f_{sl} \ll \sqrt{\alpha}$. From the first condition, it can be inferred from narrowband modulation theory that the maximum frequency component in $S_\epsilon(f)$ is approximately $f_{max} \approx f_{sl}$. Thus, the second condition, $f_{sl} \ll \sqrt{\alpha}$, amounts to condition (3.39), and we the "narrowband" compensation algorithm to be effective as well as the "wideband" one. We also note that for the parameters of our simulation, the time-bandwidth product is $BT = 25,000 \gg 1$, so that (3.47) for all cases simulated here.

With α = 100 GHz/s as specified in Table 4, $\sqrt{\alpha} \approx$ 316 kHz. We have chosen f_{sl} well below that, at $f_{sl} = 4$ kHz, and have chosen A_{sl} = 0.1. The simulated range profiles with these parameters are shown in **Error! Reference source not found.**.
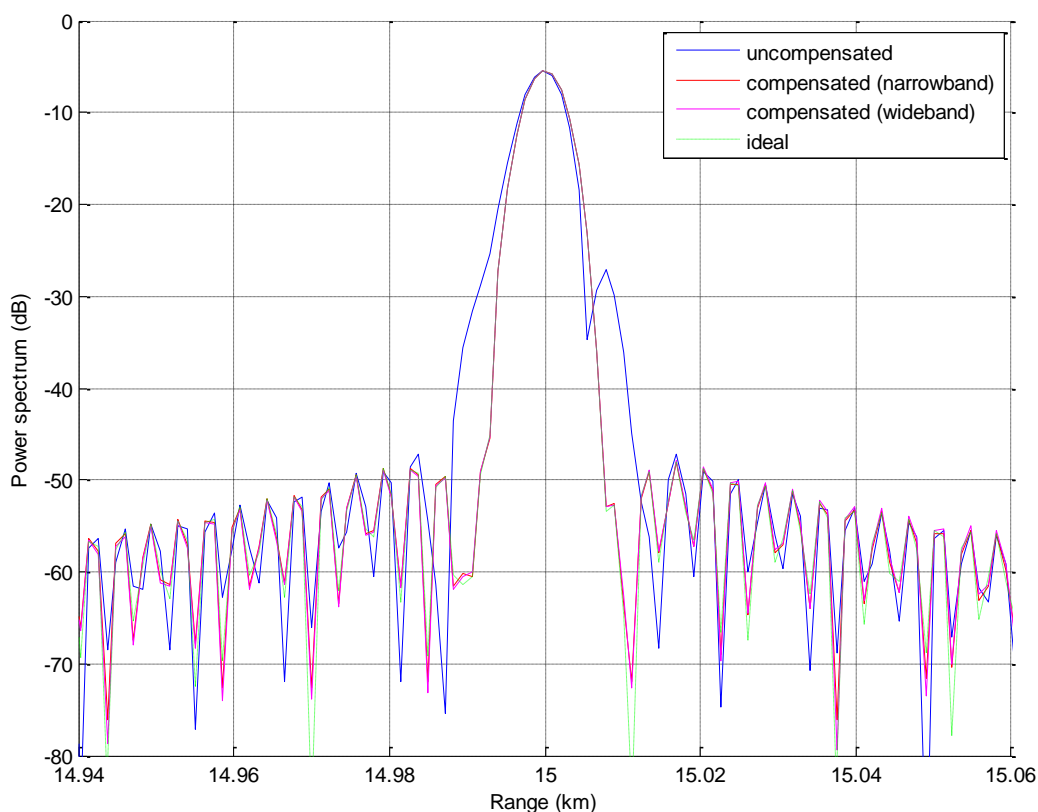
Figure 19 Simulated range profiles for a sinusoidal phase error with A_{sl} = 0.1 radians and f_{sl} = 4 kHz. The beat frequency has been converted to range in accordance with the relation $R = (cT/2B)f_b$. The power spectrum is expressed in decibel relative to the peak signal power obtainable without phase errors or windowing.

As seen from Figure 19, the "uncompensated" or "raw" IF signal (blue line) perturbed by the sinusoidal phase errors exhibits two 'paired echoes' spaced $(cT/2B)f_{sl}$ = 6 meters from the desired target beat signal at R = 15 km. The left paired echo is not resolved, whereas the right one does produce a distinct peak which could be misinterpreted as a second target. (The lack of symmetry of the target response is due to the range-dependent phase terms, which could different degrees of spectral interference with the main lobe for both sidelobes). The "narrowband" (red line) and "wideband" (magenta line) compensated signals, however, agree very well with the ideal target response (green dashed line) and each other.

4.4.1.2 *High-frequency phase error ($f_{sl} \cong \sqrt{\alpha}$)*

We have repeated the above simulation for the same phase error amplitude, $A_{sl} = 0.1$ radian, but a higher sidelobe ripple frequency: $f_{sl} = 0.2\sqrt{\alpha} \approx 63$ kHz. The resulting simulated range profile is shown below in Figure 20.
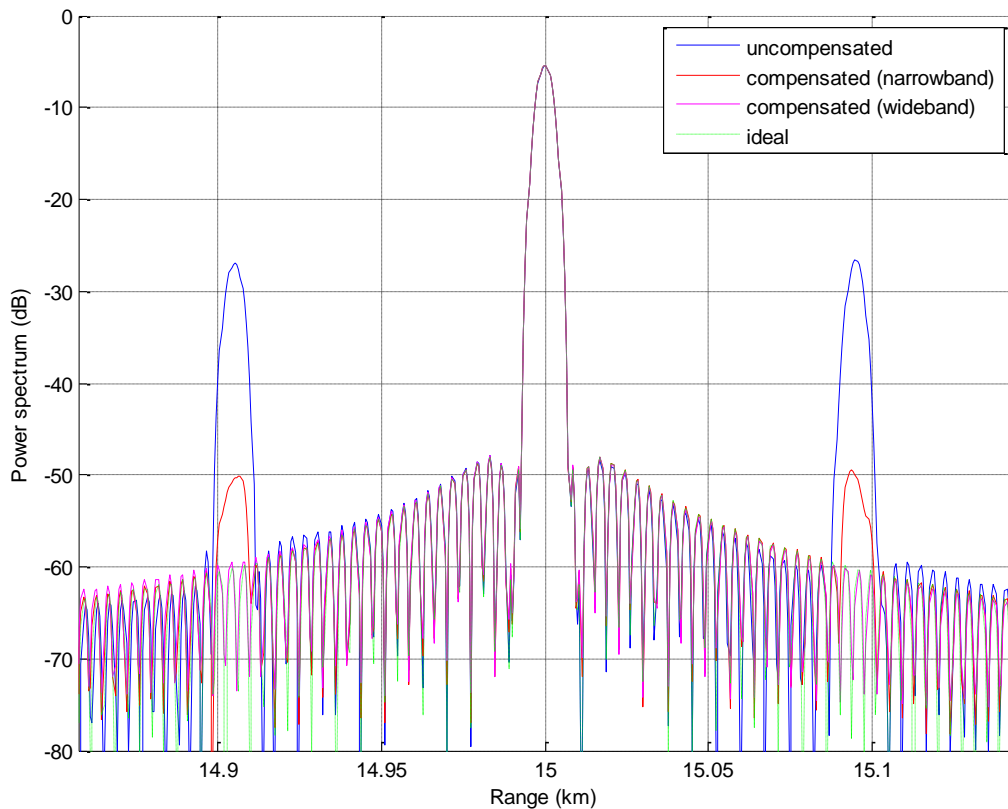
Figure 20 Simulated range profile with $A_{sl} = 0.1$ and $f_{sl} = 0.2\sqrt{\alpha} \approx 63$ kHz.

As seen from Figure 20, for $f_{sl} = 0.2\sqrt{\alpha}$, the "narrowband" method of Burgos-Garcia et al. {Burgos-Garcia, 2003 #341} (red line) is still somewhat effective in reducing sidelobe levels, but is far less effective than the "wideband" method of Meta {Meta, 2007 #46}. This can be explained by the fact that condition (3.39) is "starting to get" violated.

4.4.2   Power-law phase errors

In Section 2.2.1.2, we maintained that a *linear* phase error compensation algorithm which worked for sinusoidal phase errors should work for general phase errors as well. In this section, we perform simulations for power-law phase errors which confirm this statement.

4.4.2.1   Cubic phase error

We have simulated the phase error

$$2\pi\epsilon(t) = k_3 t^3 \tag{4.29}$$

with $k_3 = 10/(\tau T^2) = 4 \times 10^{11}$ Hz/s^2. The resulting simulated range profile is shown in Figure 21.

Figure 21 Simulated range profile for a cubic phase error.

The cubic phase error in the transmitted signal leads to a quadratic phase error in the beat signal – in other words, the beat signal is chirped. As discussed by Soumekh {Soumekh, 1999 #218}, this leads to a symmetric 'spreading' of the range profile energy. It is seen from Figure 21, both the "wideband" and the "narrowband" compensation method are very effective in removing the phase errors.

4.4.2.2   *Quartic phase errors*
We have simulated the phase error

$$2\pi\epsilon(t) = k_4 t^4 \tag{4.30}$$

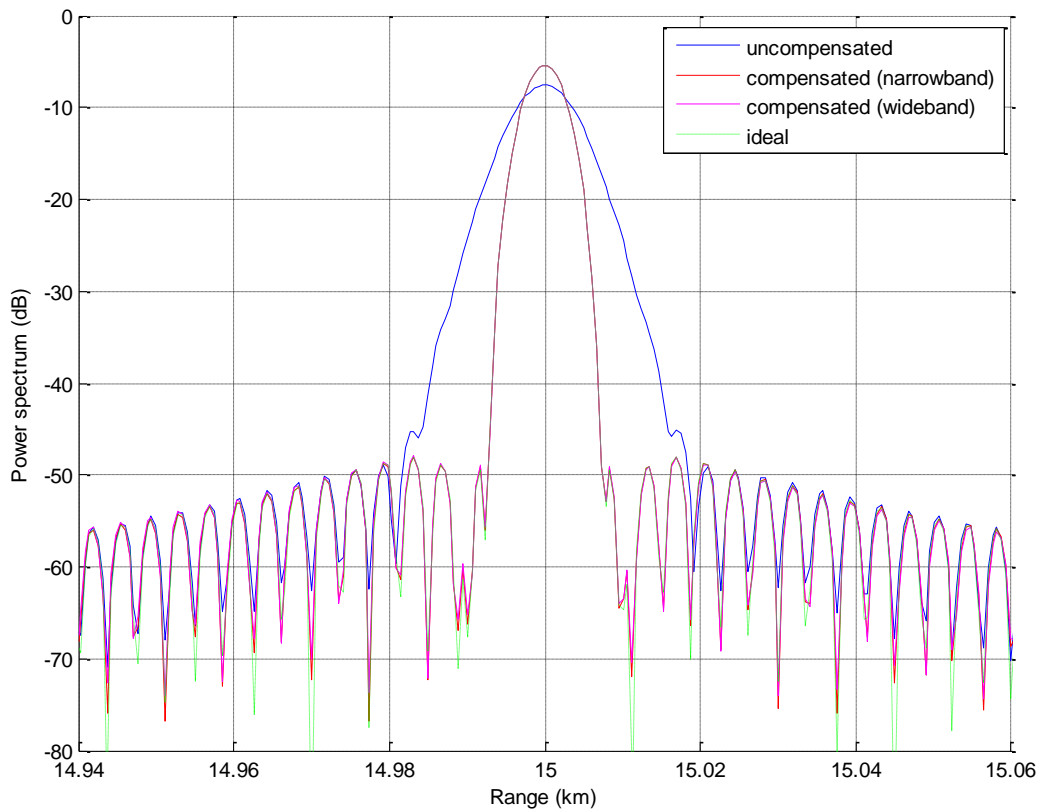with $k_4 = 10/(\tau T^3) = 8 \times 10^{14}$ Hz/s^3. The resulting simulated range profile is shown in Figure 21.
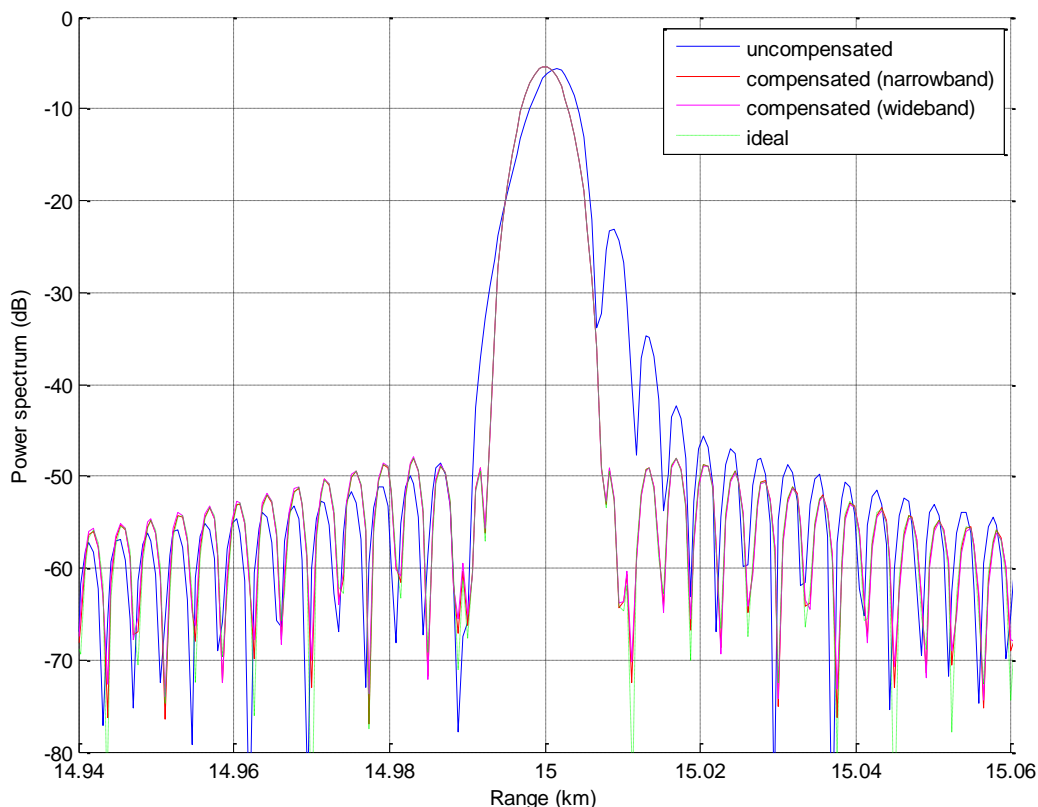
Figure 22 Simulated range profile with quartic phase errors.

A quartic phase error in the transmitted signal gives rise to a cubic phase error in the beat signal. Thus, the beat signal is nonlinearly chirped, which gives rise to the asymmetric point target response shown above {Soumekh, 1999 #218}. Both the "wideband" and "narrowband" compensations are again effective in this case.

4.5   Concluding remarks

To summarize, we have simulated both the "wideband" and "narrowband" phase error compensation algorithms, and found that "narrowband" algorithm provides effective compensation of low-frequency phase errors, while the "wideband" algorithm also works well for high-frequency phase errors.

In our implementation of the "wideband" algorithm, the suppression of 'paired echoes' was found to be better if we applied a deskew filter to the phase error function s_ϵ, instead of a skew filter as derived in Section 3.4, which is apparently at odds with our analytical development in Chapter 3.

This does not necessarily imply that our derivation is incorrect, however. As shown in Section 3.5.2, if we apply a deskew filter to a time-limited phase-modulated signal (in our case, s_{IF2}), then due to the different group delays of the 'paired echoes', the interval on which the deskew filter output matches that for a temporally infinite phase-modulated signal is *shorter* than the duration of the original signal. In other words, "edges" of the original interval are "contaminated" by artifacts due to the time-limited nature of s_{IF2}. However, in our simulations, we have not taken into account this

effect, and have performed the spectral analysis over the entire sweep period in all cases[20]. Further work must be carried out to ascertain what the effect of the "contaminated edges" is.

---

[20] In any case, the portion affected by this "contamination" is small; for example, for the parameters in the example in Section 4.4.1.2 where $f_{sl} = 0.2\sqrt{\alpha}$, the relative group delay of the "upper and lower sidelobes" relative to the main target signal is only $f_{sl}/\alpha \approx 0.63$ μs, or 0.13% of the sweep period. However, the amplitudes of the remaining sidelobes after applying the phase error compensation algorithm with a skew filter in the last step is of the same order of magnitude.

5 Estimation of the phase errors

In the development of the phase error compensation algorithm, it was assumed that the phase error term $\epsilon(t)$ was known. In this section, we overcome this assumption and describe how to estimate $\epsilon(t)$ directly from the deramped data.

In Section 5.1, we review a known method of determining the error function using a reference delay.

5.1 Review of a known method using a reference delay

One way to measure the phase error in linear frequency-modulated (LFM) radar systems, first described by Withers {Withers, 1966 #389} and also applied by Meta {Meta, 2007 #364}, uses a reference response with delay τ_{ref}, which is usually implemented using a delay line. The IF signal corresponding to this reference response is

$$s_{IF}(t) = \exp\left[j2\pi\left(f_c\tau_{ref} + \alpha\tau_{ref}t - \frac{1}{2}\alpha\tau_{ref}^2 + \epsilon(t) - \epsilon(t - \tau_{ref})\right)\right]. \tag{4.31}$$

For small delays, we can approximate the phase error in the IF signal as

$$\epsilon(t) - \epsilon(t - \tau_{ref}) \approx \tau_{ref}\epsilon'(t), \tag{4.32}$$

where $\epsilon'(t)$ denotes the derivative of $\epsilon(t)$ with respect to time. This relation is also the basis of the resampling methods to compensate frequency sweep non-linearity {Vossiek, 1998 #390}; in this case, however, we require (4.32) to hold *only* for the reference delay τ_{ref}, and not for every τ in the range window of interest.

We thus obtain an estimate, $\tilde{\epsilon}'(t)$, for $\epsilon'(t)$ as follows:

$$\tilde{\epsilon}'(t) = \frac{\epsilon(t) - \epsilon(t - \tau_{ref})}{\tau_{ref}}. \tag{4.33}$$

Integrating (4.33), we find a phase error estimate

$$\tilde{\epsilon}(t) = \int^t \tilde{\epsilon}'(u)\, du + \text{constant}. \tag{4.34}$$

The constant phase is of no consequence for the power spectrum of the beat signal.

A problem with the 'reference delay' method is that we have two conflicting requirements. On one hand, we would like to choose τ_{ref} small, so that (4.32) yields a good approximation of the derivative $\epsilon'(t)$. On the other hand, however, if τ_{ref} is small, the differential phase error $\epsilon(t) - \epsilon(t - \tau_{ref})$ is small, and could easily be swamped by stochastic phase errors. It would seem advantageous to deduce $\epsilon(t)$ by observing the beat signals for larger target delays, when the effects of the phase errors are more conspicuous. Moreover, it seems intuitive that there is something to be learned from how the phase errors *develop* with increasing τ.

5.2 Proposal of a novel method using ambiguity functions

In this section, we propose a novel method for estimating the phase error in the transmit signal $\epsilon(t)$ from the deramped data observed for different ranges.

If we consider the beat signal spectrum $S_{IF}(f)$ to be a function of τ as well, we can write it in the form

$$S_{IF}(\tau,f) = \int_{-\infty}^{\infty} s_{TX}(t)s_{TX}^*(t-\tau)\exp(-j2\pi ft)\,dt. \tag{4.35}$$

Now, suppose that $s_{TX}(t)$ can be expressed as follows:

$$s_{TX}(t) = u(t)\exp(j2\pi f_c t), \tag{4.36}$$

where $u(t)$ is called the *waveform* of the transmitted signal and f_c its *carrier frequency*. Then (4.35) has the form

$$S_{IF}(\tau,f) = \exp(j2\pi f_c\tau)\int_{-\infty}^{\infty} u(t)u^*(t-\tau)\exp(-j2\pi ft)\,dt. \tag{4.37}$$

Defining $\chi(\tau,f) = S_{IF}(\tau,f)\exp(-j2\pi f_c\tau)$, this can be written as

$$\chi(\tau,f) = \int_{-\infty}^{\infty} u(t)u^*(t-\tau)\exp(-j2\pi ft)\,dt. \tag{4.38}$$

The function $\chi(\tau,f)$ is called the *ambiguity function* of $u(t)$. Thus, the problem of determining the transmitted signal $s_{TX}(t)$ from the spectrum of the IF signal, $S_{IF}(\tau,f)$, is equivalent to that of determining a function $u(t)$ from its ambiguity function $\chi(\tau,f)$.

The latter problem was discussed by Wilcox {Wilcox, 1991 #391}. An important aspect here, though, is that not all functions of two variables (τ and f) are ambiguity functions: the ambiguity functions are a *subspace* of the space of all functions of two variables. (In fact, Wilcox shows that a basis for the subspace of ambiguity functions $\chi(\tau,f)$ can be obtained from the cross-ambiguity functions of a family of orthogonal basis functions for the space of waveforms, $u(t)$). Wilcox also describes a method to *project* a given function of two variables onto the space of ambiguity functions.

Now, consider a series of measurements $S_{IF}(\tau,f)$ from which we want to determine the waveform $u(t)$ – and hence, the phase error function $s_\epsilon(t)$. Suppose the measurements are perturbed by other errors, which as stochastic errors or errors incurred in the receive signal chain, which are not attributable to an error in the transmitted frequency sweep. These "other" phase errors generally do not give rise to ambiguity functions, and will be "filtered out" when the measured data $S_{IF}(\tau,f)$ is projected onto the space of ambiguity functions in order to determine $u(t)$. Hence, we expect the method of Wilcox to more robust in the presence of other sources of error.

Needless to say, more simulation work must be done to validate the ideas laid out above, which unfortunately was no longer available within the period

6 Conclusions and discussion

The nonlinearity of the frequency sweep is a limiting factor for the performance of linear FMCW radars in many applications. In this thesis, we have studied methods devised by Burgos-Garcia et al. {Burgos-Garcia, 2003 #341} and Meta et al. {Meta, 2007 #46} to compensate for such nonlinearities by digital post-processing of the deramped signal.

To summarize, in this thesis we make the following accomplishments and contributions to knowledge:

- We derive the phase error compensation algorithm for "wideband" signals, and find a discrepancy with the algorithm as originally presented by Meta {Meta, 2007 #46} in that in our method, the phase error function $s_\epsilon(t)$ is "skewed" (Fresnel transformed), to obtain the correction function to remove the residual phase errors in the last step, whereas in Meta's algorithm $s_\epsilon(t)$ is "deskewed" (inverse Fresnel transformed) for that purpose. We derive our version of the algorithm in two different ways, one set in the frequency domain and one in the time domain, and check it for a small-angle sinusoidal phase error.

- We show that the algorithm of Meta, which is applicable for wideband IF signals, reduces to the algorithm of Burgos-Garcia in the case of narrowband IF signals.

- We simulate both algorithms, and shown that they are effective within their underlying assumptions.

- We propose a novel method for determining phase errors which, by projecting the IF signal spectrum observed at different ranges onto the space of ambiguity functions for the waveform of the transmitted signal, should provide more robust measurement of the transmitted sweep nonlinearities in the presence of other sources of error.

The findings of this thesis could have major technological implications. The existence of these algorithms means that transmitted frequency sweeps need not necessarily be linear, which in turn means that all the hardware techniques devised for generating linear sweeps could become obsolete.

Removing the requirement that sweeps must be linear also has major implications for electronic warfare. If an intercept receiver knows what type of radar signals to expect (for example, linear chirps), it can devise processing methods to increase its processing gain, reducing the processing gain advantage of the FMCW radar and thereby jeopardizing the radar's tactical advantage. If the transmitted sweep no longer has to be linear, however, the ability of intercept receivers to achieve such processing gain is reduced, and the low probability of intercept (LPI) property of FMCW radars maintained.

Bibliography

Adamy, D. (2001). EW 101: a first course in electronic warfare. Norwood, MA, Artech House.

Adamy, D. (2004). EW 102: A Second Course in Electronic Warfare, Horizon House Publications, Inc.

Barrick, D. E. (1973). FM/CW Radar Signals and Digital Processing.

Beasley, P. and D. Lawrence (2006). Frequency Modulated Continuous Wave (FMCW) Radar Having Improved Frequency Sweep Linearity. Q. Ltd.

Beasley, P. D. L. (2009). Coherent Frequency Modulated Continuous Wave Radar. U. S. P. Office.

Beasley, P. D. L., A. G. Stove, et al. (1990). Solving the problems of a single antenna frequency modulated CW radar. Radar Conference, 1990., Record of the IEEE 1990 International.

Boashash, B. (1992). "Estimating and interpreting the instantaneous frequency of a signal. I. Fundamentals." Proceedings of the IEEE **80**(4): 520-538.

Bracewell, R. N. (1986). The Fourier transform and its applications, McGraw-Hill.

Brooker, G. M. (2005). Understanding Millimetre-Wave FMCW Radars. 1st International Conference on Sensing Technology. Palmerston North, New Zealand**:** 152-157.

Burgos-Garcia, M., C. Castillo, et al. (2003). "Digital on-line compensation of errors induced by linear distortion in broadband LFM radars." Electronics Letters **39**(1): 116-118.

Caputi, W. J. (1971). "Stretch: A Time-Transformation Technique." Aerospace and Electronic Systems, IEEE Transactions on **AES-7**(2): 269-278.

Carrara, W. G., R. S. Goodman, et al. (1995). Spotlight Synthetic Aperture Radar: Signal Processing Algorithms, Artech House.

Carson, J. R. (1922). "Notes on the Theory of Modulation." Proceedings of the IRE **10**(1): 57-64.

Chen, V. C. and H. Ling (2002). Time-Frequency Transforms for Radar Imaging and Signal Analysis, Artech House.

Cooley, J., P. Lewis, et al. (1967). "Application of the fast Fourier transform to computation of Fourier integrals, Fourier series, and convolution integrals." Audio and Electroacoustics, IEEE Transactions on **15**(2): 79-84.

Eichel, P. H. (2005). IFP V4.0: A Polar-Reformatting Image Formation Processor for Synthetic Aperture Radar, Sandia National Laboratories.

Fuller, K. L. (1990). "To see and not be seen [radar]." Radar and Signal Processing, IEE Proceedings F **137**(1): 1-10.

Gori, F. (1994). Why is the Fresnel Transform So Little Known? Current Trends in Optics. J. C. Dainty, Academic Press.

Griffiths, H. D. (1990). "New ideas in FM radar." Electronics & Communication Engineering Journal **2**(5): 185-194.

Griffiths, H. D. (1991). The effect of phase and amplitude errors in FM radar. High Time-Bandwidth Product Waveforms in Radar and Sonar, IEE Colloquium on.

Griffiths, H. D. and W. J. Bradford (1992). "Digital generation of high time-bandwidth product linear FM waveforms for radar altimeters." Radar and Signal Processing, IEE Proceedings F **139**(2): 160-169.

Gurgel, K. W. and T. Schlick (2009). Remarks on Signal Processing in HF Radars Using FMCW Modulation. International Radar Symposium IRS 2009. Hamburg, Germany**:** 63-67.

Harris, F. J. (1978). "On the use of windows for harmonic analysis with the discrete Fourier transform." Proceedings of the IEEE **66**(1): 51-83.

Jakowatz, C. V., D. E. Wahl, et al. (1996). Spotlight-Mode Synthetic Aperture Radar: A Signal Processing Approach, Kluwer Academic Publishers.

James, G. L. (2003). Geometrical Theory of Diffraction for Electromagnetic Waves, Peter Peregrinus Ltd.

Keller, J. B. (1962). "Geometrical Theory of Diffraction." J. Opt. Soc. Am. **52**(2): 116-130.

Klauder, J. R., Price, A.C., Darlington, S., and Albersheim, W.J. (1960). "The Theory and Design of Chirp Radars." Bell. Syst. Tech. J. **39**(4): 745-809.

Levanon, N. and E. Mozeson (2004). Radar Signals, John Wiley & Sons.

Meta, A. (2007). Frequency Modulated Continuous Wave Radar and Synthetic Aperture Radar. N. O. v. T.-N. O. (TNO) and E. B.V.

Meta, A., P. Hoogeboom, et al. (2006). Range Non-linearities Correction in FMCW SAR. Geoscience and Remote Sensing Symposium, 2006. IGARSS 2006. IEEE International Conference on.

Meta, A., P. Hoogeboom, et al. (2007). Signal processing for FMCW SAR, Ieee-Inst Electrical Electronics Engineers Inc.

Meta, A., P. Hoogeboom, et al. (2007). "Signal Processing for FMCW SAR." Geoscience and Remote Sensing, IEEE Transactions on **45**(11): 3519-3532.

Morgan, G. D., P. D. Beasley, et al. (2006). Design considerations for a millimetric front-end for FMCW radar. MM-Wave Products and Technologies, 2006. The Institution of Engineering and Technology Seminar on.

Nalezinski, M., M. Vossiek, et al. (1997). Novel 24 GHz FMCW front-end with 2.45 GHz SAW reference path for high-precision distance measurements. Microwave Symposium Digest, 1997., IEEE MTT-S International.

Oppenheim, A. V., R. W. Schafer, et al. (1999). Discrete-time signal processing, Prentice-Hall.

Pace, P. E. (2004). Detecting and classifying low probability of intercept radar, Artech House.

Papoulis, A. (1977). Signal Analysis, McGraw-Hill.

Papoulis, A. (1994). "Pulse compression, fiber communications, and diffraction: a unified approach." J. Opt. Soc. Am. A **11**(1): 11.

Papoulis, A. (1994). "Pulse compression, fiber communications, and diffraction: a unified approach." J. Opt. Soc. Am. A **11**(1): 3-13.

Pichler, M., A. Stelzer, et al. (2003). Influence of Systematic Frequency-Sweep Non-Linearity on Object Distance Estimation in FMCW/FSCW Radar Systems. European Microwave Conference, 2003. 33rd.

Piper, S. O. (1993). Receiver frequency resolution for range resolution in homodyne FMCW radar. Telesystems Conference, 1993. 'Commercial Applications and Dual-Use Technology', Conference Proceedings., National.

Piper, S. O. (1995). Homodyne FMCW radar range resolution effects with sinusoidal nonlinearities in the frequency sweep. Radar Conference, 1995., Record of the IEEE 1995 International.

Pozar, D. M. (2005). Microwave Engineering, John Wiley & Sons, Inc.

Press, W. H., S. A. Teukolsky, et al. (2007). Computing Fourier Integrals Using the FFT. Numerical Recipes - The Art of Scientific Computing, Cambridge University Press.

Pun, K. P., J. E. d. Franca, et al. (2003). Circuit Design for Wireless Communications - Improved Techniques for Image Rejection in Wideband Quadrature Receivers, Kluwer Academic Publishers.

Rader, C. M. (1984). "A Simple Method for Sampling In-Phase and Quadrature Components." Aerospace and Electronic Systems, IEEE Transactions on **AES-20**(6): 821-824.

Rice, D. W. and K. H. Wu (1982). "Quadrature Sampling with High Dynamic Range." Aerospace and Electronic Systems, IEEE Transactions on **AES-18**(6): 736-739.

Richards, M. A., J. A. Scheer, et al. (2010). Principles of Modern Radar, SciTech Publishing, Inc.

Richter, J. H., D. R. Jensen, et al. (1973). "New Developments in FM-CW Radar Sounding." Boundary-Layer Meterology **4**: 179-199.

Ross, R. A. and M. E. Bechtel (1968). "Scattering-Center Theory and Radar Glint Analysis." Aerospace and Electronic Systems, IEEE Transactions on **AES-4**(5): 756-762.

Scheer, J. A. (1993). Coherent Radar Performance Estimation, Artech House.

Sheehan, D. V. and H. D. Griffiths (1992). "The effect of pulse phase distortion on the height estimation of a radar altimeter." International Journal of Remote Sensing **13**(17): 3303-3310.

Skolnik, M. (2008). Radar Handbook, McGraw-Hill.

Soumekh, M. (1999). Synthetic Aperture Radar Signal Processing with MATLAB Algorithms, John Wiley & Sons.

Stove, A. G. (1992). "Linear Fmcw Radar Techniques." Iee Proceedings-F Radar and Signal Processing **139**(5): 343-350.

Stove, A. G., A. L. Hume, et al. (2004). "Low probability of intercept radar strategies." Radar, Sonar and Navigation, IEE Proceedings - **151**(5): 249-260.

Strauch, R. G. (1976). Theory and Application of the FM-CW Doppler Radar. Department of Electrical Engineering. Boulder, University of Colorado. **Ph.D.**

Waters, W. M. and B. R. Jarrett (1982). "Bandpass Signal Sampling and Coherent Detection." Aerospace and Electronic Systems, IEEE Transactions on **AES-18**(6): 731-736.

Willis, N. J. and H. D. Griffiths (2007). Advances in Bistatic Radar, SciTech Publishing, Inc.

Appendix: MATLAB simulation code

We have implemented the phase error compensation in MATLAB. Below, we present a listing of our code.

```
1    fc=10e9;                  % center frequency (10 GHz)
2    B=50e6;                   % chirp bandwidth (50 MHz)
3    T=500e-6;                 % chirp period (500 us)
4    alpha=B/T;                % chirp rate (100 GHz/s)
5
6    R=15e3;                   % target range 15 km
7    c=3e8;                    % speed of light
8    tau=2*R/c;                % target transit time 100 us
9    fb=alpha*tau;             % beat frequency 10 MHz
10
11   fs=25e6;                  % sampling frequency 25 MHz
12   Ts=1/fs;                  % sampling period (40 ns)
13   N=T/Ts;                   % number of samples per sweep (12,500)
14   Np=(T-tau)/Ts;            % number of processed samples per sweep (10,000)
15
16   A=alpha/fs^2;             % dimensionless chirp parameter
17
18   % Phase error function
19   Asl=0.5;                       % phase error amplitude (radian)
20   fsl=.1*sqrt(alpha);            % phase error frequency
21   e=@(t) Asl*cos(2*pi*fsl*t); % phase error
22   se=@(t) exp(1j*e(t));       % error function
23
24   % Generation of the beat signal
25   phiTX=@(t) 2*pi*(fc*t+1/2*alpha*t.^2)+e(t);        % transmit signal phase
26   phib=@(t) phiTX(t)-phiTX(t-tau);                   % beat signal phase
27   r=@(t) rectpuls((t-tau/2)/(T-tau));                % observation window
28   sb=@(t) r(t).*exp(1j*phib(t));                     % complex beat signal
29
30   % Time and frequency grids
31   n=0:N-1;                          % time index
32   t=(-N/2+n)*Ts;                    % time grid
33   NFFT=2^nextpow2(N+1/A);           % choose the number of FFT points same
34   as for deskew filter processing
35   k=0:NFFT-1;                       % frequency index
36   f=(-NFFT/2+k)/NFFT*fs;            % frequency grid
37
38   % Phase error compensation algorithm
39   sIF=sb(t);                        % sampled beat signal
40   sIF2=sIF.*conj(se(t));            % remove transmitted phase errors sIF2
41   sIF3=deskew(sIF2,A);              % deskew filter to obtain sIF3
42   sIF4n=sIF3.*se(t);                % sIF4 (narrowband IF)
43   sea=deskew(se(t),A);              % residual phase error function
44   sIF4w=sIF3.*sea;                  % sIF4 (wideband IF)
45
46   % Calculate spectra
47   sIFd=@(t) r(t).*exp(1j*2*pi*(fc*tau-1/2*alpha*tau^2+alpha*tau*t));  % ideal
48   beat signal
49   wIF=[zeros(1,N-Np) hamming(Np,'periodic')'];                       %
50   window for sIF
51   SIFd=T/N*exp(1j*pi*N*(-1/2+k/NFFT)).*fft(wIF.*sIFd(t).*(-1).^n,NFFT);   %
52   SIF (ideal)
53   SIF=T/N*exp(1j*pi*N*(-1/2+k/NFFT)).*fft(wIF.*sIF.*(-1).^n,NFFT);        %
54   SIF (observed)
```

```matlab
55  wIF4=[hamming(Np,'periodic')' zeros(1,N-Np)];                    %
56  window for sIF4
57  SIF4n=T/N*(-1).^(N*(-1/2+k/NFFT)).*fft(wIF4.*sIF4n.*(-1).^n,NFFT);  % SIF4
58  (narrowband IF)
59  SIF4w=T/N*(-1).^(N*(-1/2+k/NFFT)).*fft(wIF4.*sIF4w.*(-1).^n,NFFT);  % SIF4
60  (wideband IF)
61
62  % Convert to normalized decibel scale
63  SIFd_dB=20*log10(abs(SIFd)/(T-tau));
64  SIF_dB=20*log10(abs(SIF)/(T-tau));
65  SIF4n_dB=20*log10(abs(SIF4n)/(T-tau));
66  SIF4w_dB=20*log10(abs(SIF4w)/(T-tau));
67
68  % Plot results
69  figure(1); hold on; grid on
70  fMHz=f/1e6;                                    % frequency in MHz
71  plot(fMHz,SIFd_dB,'g')                         % ideal signal
72  plot(fMHz,SIF_dB)                              % original IF signal
73  plot(fMHz,SIF4n_dB,'k')                        % compensated signal
74  (narrowband approximation)
75  plot(fMHz,SIF4w_dB,'m:')                       % compensated signal (wideband
76  approximation)
77  scale=1.5*fsl*T;                               % frequency offset for axis
78  limits
79  xlim([fb-scale/T fb+scale/T]/1e6)              % frequency axis limits
80  xlabel('frequency (MHz)'); ylabel('amplitude spectrum (dB)')
81  legend('s_I_F (ideal)','s_I_F','s_I_F_4 (narrowband IF method)','s_I_F_4
82  (wideband IF method)')
83  ylim([-80 0])
```

A short explanation of the code follows. In lines 1-14, we define the parameters of the simulation in accordance with Table 4 in Section 4.3. In line 16, we define the dimensionless chirp parameter $A = \alpha/f_s^2$ in accordance with equation (4.25). In lines 19-22, we define the phase error function. In lines 25-28, we generate the beat signal using the chirp parameters and phase error function defined above. In lines 39-59, we implement the flow diagram depicted in Figure 18. Finally, in lines 63-83, we plot the results.